Journal of Molecular Structure 1257 (2022) 132630

Contents lists available at ScienceDirect

Journal of Molecular Structure

journal homepage: www.elsevier.com/locate/molstr

A versatile study of novel A_3B-type unsymmetric zinc(II) phthalocyanines containing thiazolidin-4-one: Their, carbonic anhydrase I, II isoenzymes, and xanthine oxidase inhibitors evaluation

Emel Karakılıç[a], Zuhal Alım[b], Aslıhan Günel[b], Arif Baran[a,*]

[a] Department of Chemistry, Faculty of Arts and Sciences, Sakarya University 54050 Sakarya, Turkey
[b] Department of Chemistry Faculty of Science and Arts, Kırşehir Ahi Evran University 40100 Kırşehir, Turkey

ARTICLE INFO

Article history:
Received 30 December 2021
Revised 9 February 2022
Accepted 11 February 2022
Available online 15 February 2022

Keywords:
Thiazolidin-4-one
Symmetrical phthalocyanines
Unsymmetrical phthalocyanines
Voltammetry
Carbonic anhydrase i
II
Xanthine oxidase

ABSTRACT

In this study, four novel phthalocyanine complexes containing zinc metal were synthesized. After preparing the starting compounds (2-(4-hydroxyphenyl)-3-phenylthiazolidin-4-one **1** and 2-(4-(2-hydroxyethoxy)phenyl)-3-phenylthiazolidin-4-one **3** by the conventional method, they were reacted with 4-nitrophthalonitrile separately using K_2CO_3 in DMF. Compounds **2** and **4**, are well-documented compounds for obtaining phthalocyanines. Subsequently, synthesized phthalonitrile compounds **2** and **4** were reacted with Zn(II) salt at high temperature in the presence of DBU to convert them into targeted symmetrical (**2a, 4a**) and unsymmetrical (**2b, 4b**) phthalocyanines under suitable conditions. Their photochemical, photophysical, and electrochemical features were then examined. These metallophthalocyanines indicated good solubility in some organic solvents, such as DMSO, DMF, THF, DCM, and $CHCl_3$. Furthermore, the structures of ligands (**1, 2, 3, 4**) were determined by ^{1}H NMR, ^{13}C NMR, and FT-IR spectrometry, while complexes (**2a, 2b, 4a, 4b**) were determined by FT-IR, UV–Vis, fluorescence, and MALDI-TOF spectrometry. Inhibitory effects of ligand and phthalocyanine compounds (**1, 2, 3, 4, 2a, 2b, 4a, 4b**) against human erythrocyte carbonic anhydrase I (hCA I) and II (hCA II) isoenzymes, as well as cow's milk xanthine oxidase (XO), were examined. It was found that **2a, 2b, 4a**, and **4b** had strong inhibition effects at micromolar levels against all three. The compounds **2b** and **4b** showed stronger inhibition effects for hCA I and II than **2a** and **4a**. In the case of XO, although the inhibition effects of these molecules (**2b, 4a, 4b**) were similar, **2a** had the strongest inhibition effect. Since CA and XO inhibitors are the target molecules of drug development studies to be used in the treatment of many diseases, the results of this study will aid drug design studies in the development of new XO and CA inhibitors.

1. Introduction

Phthalocyanines (MPcs, Pcs), particularly analogs containing natural porphyrin rings, have been researched in many scientific and technological fields. They are planar conjugated macrocyclic molecules having 18-π electrons, aromatic compounds formed by an electron cloud between four isoindole units formed by the alternating replacement of carbon and nitrogen atoms. They exhibit multiple and reversible electron transfer properties [1–4].

MPcs and/or Pcs, which have many technological applications and upramolecular material chemistry. They have optoelectronic properties, are stable against light and chemicals, and are used as chemical catalysts [5,6–8]. Zn-containing metallophthalocyanines are recommended for PDT because of their long triplet lifetimes and efficient singlet oxygen production [9]. Recent research has focused on the biological and pharmaceutical applications of phthalocyanines. These chemical compounds have various relevant properties, including enzyme inhibition as well as antioxidant, antibacterial [10,11], anticancer [12], and antimicrobial [13] activities. For example, phthalocyanines have been investigated concerning their inhibitory effects on α-glycosidase, carbonic anhydrase, cholinesterases [11,14], and xanthine oxidase (XO) [15]. As phthalocyanines need to be easily soluble for their biological and technological applications, studies on ZnPcs containing thiazole derivatives are important [16,17]. New phthalocyanine compounds, including thiazolidines with high solubility, were tried to be synthesized in the planned study. Thiazolidines are a versatile scaffold

* Corresponding author.
E-mail address: abaran@sakarya.edu.tr (A. Baran).

https://doi.org/10.1016/j.molstruc.2022.132630
0022-2860/

for developing new bioactive structures. Moreover, they also have important biological and pharmacological properties. These include antidiarrheal, anticonvulsant, antimicrobial, antidiabetic, antihistaminic, anticancer, antidepressant, anti-HIV, antiplatelet activating factor, antioxidant, anti-inflammatory, and cyclooxygenase inhibitory properties [18–21a]. It is known that heteroatoms (such as sulfur, nitrogen, and oxygen) used as substituents have a feature that can affect the electronic spectra of the complexes. Therefore, benzothiazoles were used, considering that heteroatom-containing substituents increase the photosensitizing activities of the complexes due to the synergistic effect [21b–d]. In this work, we connected the thiazolidin-4-one units to the phthalocyanine ring to increase the pharmacological properties of and for the determination of the effects different enzymes have on substituted groups of phthalocyanines. Thus, new phthalocyanine compounds were designed from molecules formed by synthesizing thiazolidine derivatives. The inhibition activities of these thiazolidine-derived phthalocyanines against carbonic anhydrase isoforms and XO were examined in detail. Carbonic anhydrases (CA, carbonate hydrolase, carbonate dehydratase, EC 4.2.1.1) are a Zn^{2+}-containing metalloenzyme commonly found in living organisms that catalyze the reversible hydration of CO_2 [22]. They are found in vertebrates, invertebrates, higher plants, algae, and bacteria [23]. To date, 16 CA isoenzymes have been identified in vertebrates, and it has been determined that the vital functions of these isoenzymes vary according to the tissues and organs [24]. Abnormal levels or activity changes of CA isoenzymes are associated with many diseases [25], such as glaucoma [26], edema [27], central nervous system and renal diseases [28], osteoporosis [29], and cancer [30]. Therefore, it is crucial to determine inhibitors and activators specific to CA isoenzymes in the biomedical field. Numerous CA inhibitors have been developed to date, with molecules such as acetazolamide (AZA), methazolamide, dorzolamide, brinzolamide, diclofenamide, ethaxazolamide, zonisamide, and indisulam used clinically for the treatment of diseases such as hypertension, glaucoma, edema, and epilepsy [24,31,32]. Xanthine oxidase (XO: EC 1.17.3.2), in contrast, is a homodimer metalloflavoprotein commonly found in mammalian tissues [33–35]. It is the key enzyme that catalyzes the oxidation of hypoxanthine and xanthine to uric acid. It is also responsible for the formation of superoxide anions and hydrogen peroxide [35–37]. Excessive production of uric acid results in hyperuricemia, which is the basis of gout [35–38]. In addition, hydrogen peroxide and superoxide anion radicals cause severe complications, including DNA damage [35,39], cardiovascular diseases, diabetes, and kidney dysfunctions [35,40–43]. Therefore, XO inhibitors are significant in preventing uric acid accumulation and superoxide formation. Allopurinol is a strong XO inhibitor used as a treatment agent in cases of hyperuricemia. However, its use is limited due to its serious side effects [36,44]. Febuxostat and topiroxostat, molecules approved by the U.S. Food and Drug Administration, also servehttps://www.fda.gov/ as XO inhibitors. It has been observed that these molecules have serious side effects in clinical applications [36,45,46]. Therefore, it is important to identify less toxic, effective XO inhibitors that can be used in the clinic. Recent studies have shown that various phthalocyanines have an inhibitory effect on hCAI and II isoenzymes [11,15], and XO [12,15,47]. Due to the importance of CA and XO inhibitors in the field of medicinal chemistry, studies for the determination of new and isoenzyme-specific inhibitors continue intensively.

In this study, four novel phthalocyanine compounds (symmetrical and unsymmetrical) that had the same ligand but were bound differently were documented. In addition, the spectroscopic (photophysical and photochemical), voltammetric (CV), enzymatic inhibition (human erythrocyte carbonic anhydrase I [hCA I] and II [hCA II] isoenzymes and cow milk xanthine oxidase [XO]) effects of these phthalocyanine compounds were evaluated.

2. Experimental details

2.1. Materials and methods

In the study, all chemicals (such as 4-nitrophthalonitrile, 4-hydroxybenzaldehyde, thioglycolic acid, aniline, silica gel, ethylene carbonate, 1,8-diazabicyclo[5.4.0]undec–7-ene (DBU), potassium carbonate (K_2CO_3), $Zn(CH_3COO)_2{\cdot}2H_2O$ and tetrabutylammonium hexafluorophosphate ($TBAPF_6$)) and solvents (such as N, N-dimethylformamide (DMF), tetrahydrofuran (THF), dichloromethane (DCM), dimethyl sulfoxide (DMSO), n-hexane, chloroform, methanol, ethanol, and toluene) used for the synthesis of the compounds were commercially obtained from Sigma-Aldrich and Merck. All chemicals used in enzyme inhibition studies were purchased from Sigma-Aldrich Co. (Steinheim, Germany). Thin-layer chromatography (TLC on Merck 0.2 mm silica gel 60 F_{254} analytical aluminum plates) was used for reaction controls of the synthesized compounds. Heidolph Laborota 4001 and Bibby rotary evaporator brand device was used to remove solvents. In addition, Heidolph MR Hei-standard heating stirrers were used to obtain the compounds. ^{1}H (300 MHz) and ^{13}C NMR (75 MHz) spectra were recorded using a Varian 300-MHz Mercury Plus. Infrared spectra were recorded with a Perkin-Elmer 1600 FT-IR (4000–400 cm^{-1}) spectrometer. UV–Vis and fluorescence spectrum were measured with Shimadzu UV 2600 model spectrophotometer and the Agilent Technologies Cary Eclipse spectrophotometer, respectively. The MALDI-TOF spectra were recorded with Bruker Daltonics flex Analysis (LT MALDI-TOF MS). Photo-irradiations were performed using a General Electric quartz lamp (300 W). Cyclic voltammograms of all ZnPc compounds were recorded on Gamry Interphase 1000 potentiostat with their electrode system; glassy carbon as working electrode, Pt disk as reference electrode, Pt wire as counter electrode at a scan rate of 100 mV/s and Fc/Fc^+ redox couple was utilized as external standard to calibrate the results.

2.2. Synthesis

2.2.1. Synthesis of 2-(4-hydroxyphenyl)−3-phenylthiazolidin-4-one (1)

Synthesis of starting compound 2- (4-hydroxyphenyl) −3-phenyl thiazolidin-4-one (1) was obtained according to procedure [48].

2.2.2. Synthesis of 4- (4- (4-oxo-3-phenyl thiazolidin-2-yl) phenoxy) phthalonitrile (2)

2-(4-hydroxyphenyl)−3-phenylthiazolidin-4-one 1 (0.5 g, 1.84 mmol) and 4-nitrophthalonitrile (0.32 g, 1.84 mmol) were dissolved in dry DMF (15 mL). To this mixture, anhydrous K_2CO_3 (0.46 g, 3.32 mmol) was added. The reaction mixture was heated at 50 °C under argon atmosphere for 24 h, and then the mixture is allowed to cool to room temperature. After the reaction was completed, the reaction mixture was poured into 150 mL of ice water. The residue was filtered through a filter paper and washed with plenty of water, and dried. Orange solid 4- (4- (4-oxo-3-phenylthiazolidin-2-yl) phenoxy) fthalonitrile 2 was obtained (0.45 g, 61% chemical yield). Mp: 100–102 °C. Anal. calcd for $C_{23}H_{15}N_3O_2S$: C, 69.51; H, 3.80; N, 10.57; O, 8.05; S, 8.07%; found C, 69.42; H, 3.71; N, 10.43%. FT-IR ν_{max} (cm^{-1}): 3077–3046 cm^{-1} (Ar–CH); 2232 cm^{-1} (C≡N); 1682 cm^{-1} (C = O); 1590, 1564 cm^{-1} (C = N, C = C); 1169 cm^{-1} (C–O-C). ^{1}H NMR (300 MHz, $CDCl_3$): δ ppm = 7.72 (d, J = 8.7 Hz, 1H), 7.41 (d, J = 7.6 Hz, 2H), 7.30 (m, 2H), 7.19 (m, 4H), 6.99 (d, J = 7.6 Hz, 2H), 6.16 (s, 1H), 3.95 (q, J = 5.5 Hz, 2H). ^{13}C NMR (75 MHz, $CDCl_3$): δ ppm = 171.1, 161.4, 154.2, 137.6, 137.4, 135.7, 129.8(2C), 129.5(2C), 127.7, 126.0(2C), 122.0, 121.9, 121.1(2C), 118.0, 115.5, 115.1, 109.6, 65.1, 33.7.

2.2.3. Synthesis of 2-(4-(2-hydroxyethoxy)phenyl)−3-phenyl thiazolidin-4-one (3)

2- (4-hydroxyphenyl) −3-phenylthiazolidin-4-one 1 (1 g, 3.69 mmol), ethylene carbonate (0.65 g, 7.37 mmol) and K_2CO_3 (1 g, 7.37 mmol) were dissolved in DMF. The reaction mixture was refluxed at 120 °C under argon atmosphere for 18 h and then the reaction mixture is allowed to cool to room temperature. Then mixture was poured dropwise into 100 mL of ice water. The solid was washed with plenty of water and dried. 2-(4-(2-hydroxyethoxy)phenyl)−3-phenylthiazolidin-4-one 3 was obtained in as brown solid (1 g, 86% chemical yield). Anal. calcd for $C_{17}H_{17}NO_3S$ calculated: C, 64.74; H, 5.43; N, 4.44; O, 15.22; S, 10.17%; found C, 64.97; H, 4.75; N, 4.63%. FT-IR ν_{max} (cm^{-1}): 3356 cm^{-1} (OH); 2928 cm^{-1} (Ar–H); 1668 cm^{-1} (C = O); 1596, 1510 cm^{-1} (C = N, C = C); 1076 cm^{-1} (C–O-C).^{1}H NMR (300 MHz, $CDCl_3$): δ ppm 7.32–7.16 (m, 4H), 7.14–7.10 (m, 3H), 6.79 (dm, J = 8.5 Hz 2H), 6.06 (s, 1H), 4.04 – 3.93 (m, 4H), 3.92–3.87 (m, 2H). ^{13}C NMR (75 MHz, $CDCl_3$): δ ppm = 171.5, 159.3, 137.6, 131.4, 129.3(2C), 128.9(2C), 127.4, 126.2(2C), 114.9(2C), 69.4, 65.6, 61.1, 33.8.

2.2.4. Synthesis of 4-(2-(4-(4-oxo-3-phenylthiazolidin-2-yl) phenoxy)ethoxy)phthalonitrile (4)

4-(2-(4-(4-oxo-3-phenylthiazolidin-2-yl)phenoxy) ethoxy) phthalonitrile 4 was prepared following the same procedure adopted for compound 2. The amount of reagents used are as follows: 2-(4- (2-hydroxyethoxy) phenyl) −3-phenylthiazolidin-4-on 3 (0.5 g, 1.59 mmol), 4-nitrophthalonitrile (0.27 g, 1.59 mmol), and K_2CO_3 (0.39 g, 2.85 mmol). For compound 4 (0.4 g, 57% chemical yield). Mp: 96–98 °C. Anal. calcd for $C_{25}H_{19}N_3O_3S$: C, 68.01; H, 4.34; N, 9.52; O, 10.87; S, 7.26%; found C, 67.89; H, 4.21; N, 9.47%. FT-IR ν_{max} (cm^{-1}): 2925 cm^{-1} (Ar–CH); 2231 cm^{-1} (C≡N); 1677 cm^{-1} (C = O); 1595, 1564 cm^{-1} (C = N, C = C); 1172 cm^{-1} (C–O-C). ^{1}H NMR (300 MHz, $CDCl_3$): δ ppm = 7.72 (d, J = 8.5 Hz, 1H), 7.29 (d, J = 2.5 Hz, H), 7.25 (t, J = 4.1 Hz, 3H), 7.23 (d, J = 1.8, 7.8 Hz, 2H), 7.14 (bd, J = 8.8 Hz, 2H), 6.80 (bd, J = 7.0 Hz, 2H), 6.07 (s, 1H), 4.38 – 4.36 (m, 2H), 4.30 – 4.28 (m, 2H), 3.92 (q, J = 15.8 Hz, 2H). ^{13}C NMR (75 MHz, $CDCl_3$): δ ppm = 171.6, 162.0, 158.7, 137.7, 135.5, 132.4, 129.3(3C), 128.9(3C), 127.4, 126.1(3C), 119.9, 119.8, 115.0(3C), 67.8, 66.1, 65.4, 33.8.

2.2.5. General synthesis procedure of symmetrically (2a-4a) and unsymmetrically (2b-4b) zinc (II) phthalocyanines

ZnPcs were prepared using a 3:1 ratio [49] mixture of 4-(4-(4-oxo-3-phenylthiazolidin-2-yl)phenoxy) fthalonitrile 2 (0.27 g, 0.68 mmol) and 4-(2-(4-(4-oxo-3 phenylthiazolidin-2-yl)phenoxy)ethoxy)phthalonitrile 4 (0.1 g, 0.23 mmol). $Zn(OAc)_2{\cdot}2H_2O$ (0.06 g, 0.27 mmol) were dissolved in 5 mL DMF and 1- 2 drops of DBU have added to this mixture. Then, the solution was increased up to stirred at 160 °C under nitrogen atmosphere overnight. After the reaction mixture turned green, it was monitored by Thin Layer Chromatography (TLC). When the reaction was finished, the mixture was cooled to room temperature and poured into 100 mL of ice water. The resulting green precipitate was filtered off then washed several times with distilled water, hot ethanol/methanol, respectively, and dried under vacuum. The final product was purified and separated fractions using silica gel column chromatography THF: *n*-hexane (1:3) as eluent. The order in condensation products that arrived in the column was as follows: first fraction A_4 (2a), second fraction A_3B (2b), third fraction AB_3 (4b), and fourth gave B_4 (4a) product.

A_4 type symmetrical zinc phthalocyanine (2a): Yield: 27% (0.1 g). Anal. calcd for $C_{92}H_{60}N_{12}O_8S_4Zn$: C, 66.76; H, 3.65; N, 10.15; O, 7.73; S, 7.75; Zn, 3.95%; found C, 66.64; H, 3.58; N, 9.93%. FT-IR νmax (cm^{-1}): 3065 cm^{-1} (Ar–CH); 2924, 2853 (Al. C–H); 1685 cm^{-1} (C = O); 1596, 1493 cm^{-1} (C = N, C = C); 1043 cm^{-1} (C–O-C). UV–Vis (DMF), λ_{max}, nm ($\log_\varepsilon$): 680 (4.09), 615 (3.39), 359 (3.79). MALDI-TOF MS: *m/z* [M]+ calcd. for $C_{92}H_{60}N_{12}O_8S_4Zn$: 1652.28; found [*M*+] 1652.53. R_f value: 0.67 (*n*-hexane: THF (3: 1 v/v)).

A_3B type symmetrical zinc phthalocyanine (2b): Yield: 36% (0.14 g). Anal. calcd for $C_{94}H_{64}N_{12}O_9S_4Zn$: C, 66.44; H, 3.80; N, 9.89; O, 8.47; S, 7.55; Zn, 3.85%; found C, 66.71; H, 3.65; N, 9.77%. FT-IR νmax (cm^{-1}): 3062 cm^{-1} (Ar–CH); 2921, 2840 (Al. C–H); 1685 cm^{-1} (C = O); 1596, 1467 cm^{-1} (C = N, C = C); 1044 cm^{-1} (C–O-C). UV–Vis (DMF), λ_{max}, nm ($\log_\varepsilon$): 683 (4.89), 616 (3.31), 361 (3.72). MALDI-TOF MS: *m/z* [M]+ calcd. for $C_{94}H_{64}N_{12}O_9S_4Zn$: 1699.24; found [*M*+] 1700.04. R_f value: 0.42 (*n*-hexane: THF (3: 1 v/v)).

B_4 type symmetrical zinc phthalocyanine (4a): Yield: 12% (0.05 g). Anal. calcd for $C_{100}H_{76}N_{12}O_{12}S_4Zn$: C, 65.58; H, 4.18; N, 9.18; O, 10.48; S, 7.00; Zn, 3.57%; found C, 65.33; H, 4.46; N, 9.31%. FT-IR νmax (cm^{-1}): 3042 cm^{-1} (Ar–CH); 2928, 2853 (Al. C–H); 1604 cm^{-1} (C = O); 1488, 1444 cm^{-1} (C = N, C = C); 1064 cm^{-1} (C–O-C). UV–Vis (DMF), λ_{max}, nm ($\log_\varepsilon$): 681 (4.70), 619 (3.28), 356 (3.92). MALDI-TOF MS: *m/z* [M]+ calcd. for $C_{100}H_{76}N_{12}O_{12}S_4Zn$: 1831.40; found [*M*+] 1831.43. R_f value: 0.28 (*n*-hexane: THF (3: 1 v/v)).

AB_3 type symmetrical zinc phthalocyanine (4b): Yield: 14% (0.06 g). Anal. calcd for $C_{98}H_{72}N_{12}O_{11}S_4Zn$: C, 65.86; H, 4.06; N, 9.40; O, 9.85; S, 7.17; Zn, 3.66%; found C, 65.59; H, 3.82; N, 9.27%. FT-IR νmax (cm^{-1}): 3059 cm^{-1} (Ar–CH); 2931, 2853 (Al. C–H); 1684 cm^{-1} (C = O); 1599, 1489 cm^{-1} (C = N, C = C); 1045 cm^{-1} (C–O-C). UV–Vis (DMF), λ_{max}, nm ($\log_\varepsilon$): 682 (4.97), 620 (3.24), 360 (3.71). MALDI-TOF MS: *m/z* [M]+ calcd. for $C_{98}H_{72}N_{12}O_{11}S_4Zn$: 1784.36; found [*M*+] 1787.88. R_f value: 0.33 (*n*-hexane: THF (3: 1 v/v)).

2.3. Enzyme inhibition assay

As in our previous studies, CA I and II isoenzymes were isolated from human erythrocytes by sepharose-4B-L-tyrosine sulfanilamide column chromatography, an affinity chromatography technique [22]. The purity of isoenzymes was checked using SDS-PAGE [50]. The purified hCA I and II isoenzymes were dialyzed against 0.05 M Tris-SO_4 (pH:7.4) buffer overnight then divided into 1 mL fractions and stored at −80 °C for use in inhibition studies. In the inhibition studies of hCA I and II isoenzymes, the esterase activity measurement method defined by Verpoorte et al. was used [51]. With this method, p-nitrophenyl acetate was used as the substrate. The formation of p-nitrophenol from p-nitrophenyl acetate was monitored by measuring absorbance at 348 nm at 25 °C with a spectrophotometer. The enzyme unit was calculated using the absorption coefficient (ε = 5.4 × 10^3 M^{-1} cm^{-1}) of p-nitrophenyl acetate at 348 nm [52].. The activities of hCA I and II isoenzymes were measured for at least five different concentrations of each phthalocyanine (2a, 4a, 2b, 4b) and ligand (1 and 3) molecule. The experiments were repeated in triplicate for each inhibitor concentration. The control activity of the enzyme was accepted as 100%, and activity% plots against the phthalocyanine concentration were plotted. From these graphs, IC_{50} values expressing the inhibitor concentration that reduced the enzyme's activity by half were determined. AZA was used as a standard inhibitor for hCA I and II isoenzymes. The cow milk XO used in this study was purchased from Sigma-Aldrich (XO Item No: Sigma, X4500). The XO assay was carried out according to Noro et al [53]. with some modifications. The reaction mixture (1 mL) included 50 mM potassium phosphate buffer (pH 7.5), 0.051 mM xanthine (used as substrate), and 0.024 U XO for the control reaction. The uric acid formation was monitored by measuring the absorbance at 290 nm for 3 min. A buffer and xanthine mixture were used as a blank. The activity of XO was measured for at least five different concentrations of each

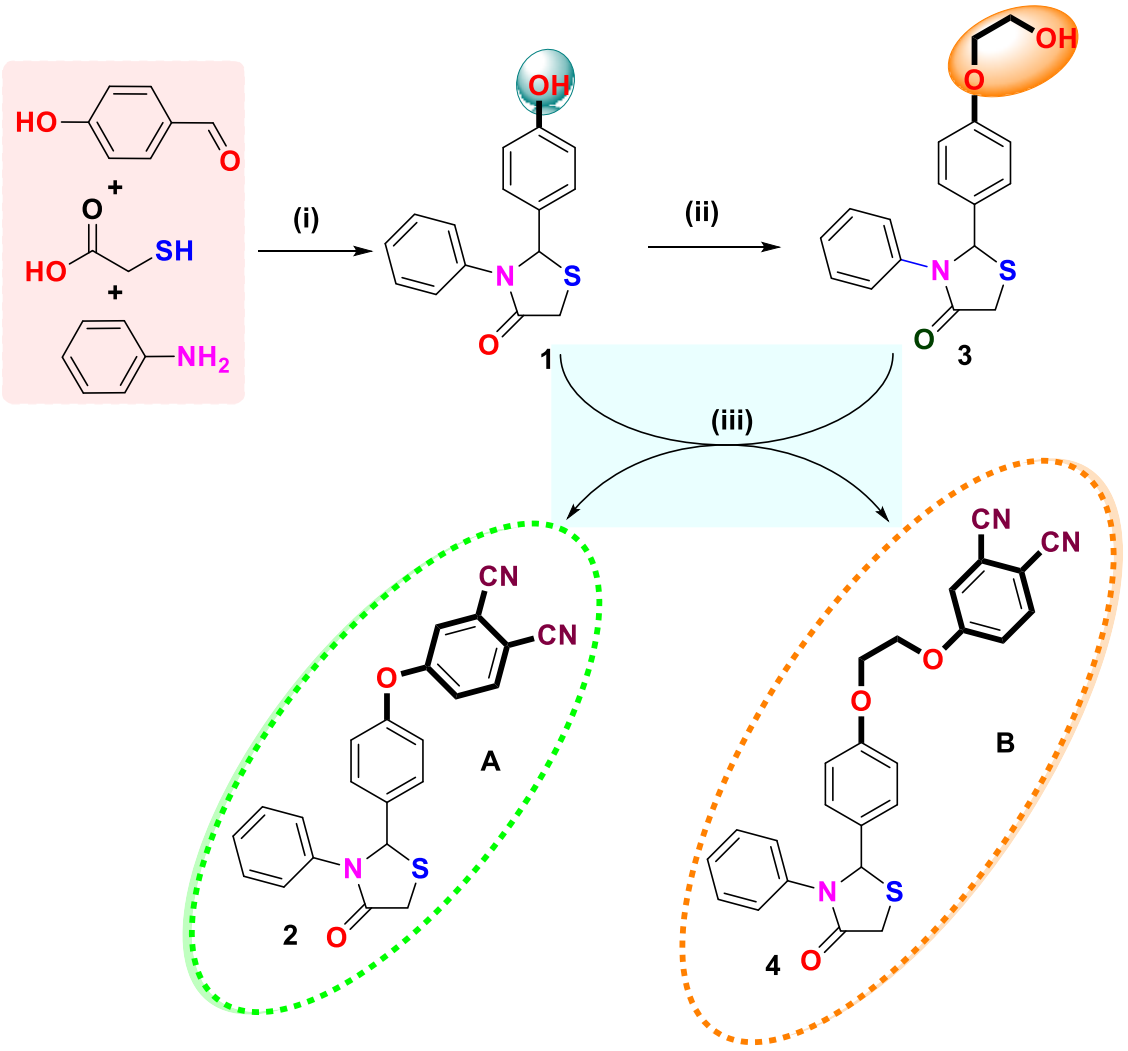

Scheme 1. Synthesis of starting compounds (1, 3) and 4-phthalonitrile derivatives (2, 4). (i) Toluene, reflux.(ii) Ethylene carbonate, K_2CO_3, DMF, 120 °C. (iii) 4-nitrophthalonitrile, K_2CO_3, DMF, 50 °C.

phthalocyanine (2a, 4a, 2b, 4b) and ligand (1 and 3). The experiments were repeated in triplicate for each inhibitor concentration. The control activity of the enzyme was accepted as 100%, and activity% plots against the phthalocyanine concentration were plotted. From these graphs, IC_{50} values expressing the inhibitor concentration that reduced the enzyme's activity by half were determined. Allopurinol was used as a standard inhibitor for XO.

3. Results and discussion

3.1. Synthesis and characterization

Various ligand systems were prepared to form peripherally symmetric and unsymmetric phthalocyanines (Pcs) with metal-binding in the present work. The main reactions involved in the synthetic route are shown in Scheme 1. The starting phthalonitrile compounds 4-(4-(4-oxo-3-phenylthiazolidin-2-yl)phenoxy)phthalonitrile 2 and 4-(2-(4-(4-oxo-3-phenylthiazolidin-2-yl)phenoxy)ethoxy)phthalonitrile 4 were synthesized and characterized according to the literature [15,54].

Statistical concentration is often utilized to synthesize phthalocyanines formed by the reaction of one different isoindole and three identical isoindole subunits (A_3B) [55]. It is known to give six possible phthalocyanine derivatives (A_4, A_3B, A_2B_2[AABB, ABAB], AB_3, B_4) by the condensation of two different phthalonitriles [56]. The stoichiometry and reactivity of precursors play an important role in the isolation of the desired A_3B type macrocycle from the mixture in statistical condensation. Here, the reactants are typically used in a 3:1 molar ratio to give forms of A_3B-type phthalocyanine [57,58]. In this study, we synthesized four possible phthalocyanine derivatives with different symmetries (A_4, B_4, A_3B,and AB_3) by the statistical concentration of different phthalonitrile ligand derivatives (1 and 3) with $Zn(OAc)_2{\cdot}2H_2O$ in DMF using DBU. A_2B_2 symmetries almost did not occur due to statistical concentration. Phthalocyanines with different symmetries and polarities were easily purified by column chromatography on silica gel using a THF/hexane (1:3) solvent system. As a result of purification, the compounds were isolated as A_4, A_3B, AB_3, and B_4, respectively.

Under these reaction conditions, the theoretical yields of products were obtained as roughly 32% (A_4 and B_4), 58% (A_3B and AB_3), and 10% (other condensation products). The synthetic procedure of newly synthesized symmetrical and unsymmetrical zinc(II) phthalocyanine derivatives (2a, 2b, 4a, and 4b) is given in Scheme 2.

All novel phthalocyanine products formed were analyzed and characterized using a series of spectroscopic techniques, including MALDI-TOF mass spectrometry, NMR (^1H and ^{13}C) and FT-IR spectroscopy, and UV–Vis spectroscopy. The FT-IR spectra of the compounds are given in Fig. S4, Fig. S8, Fig. S10, Fig. S12,

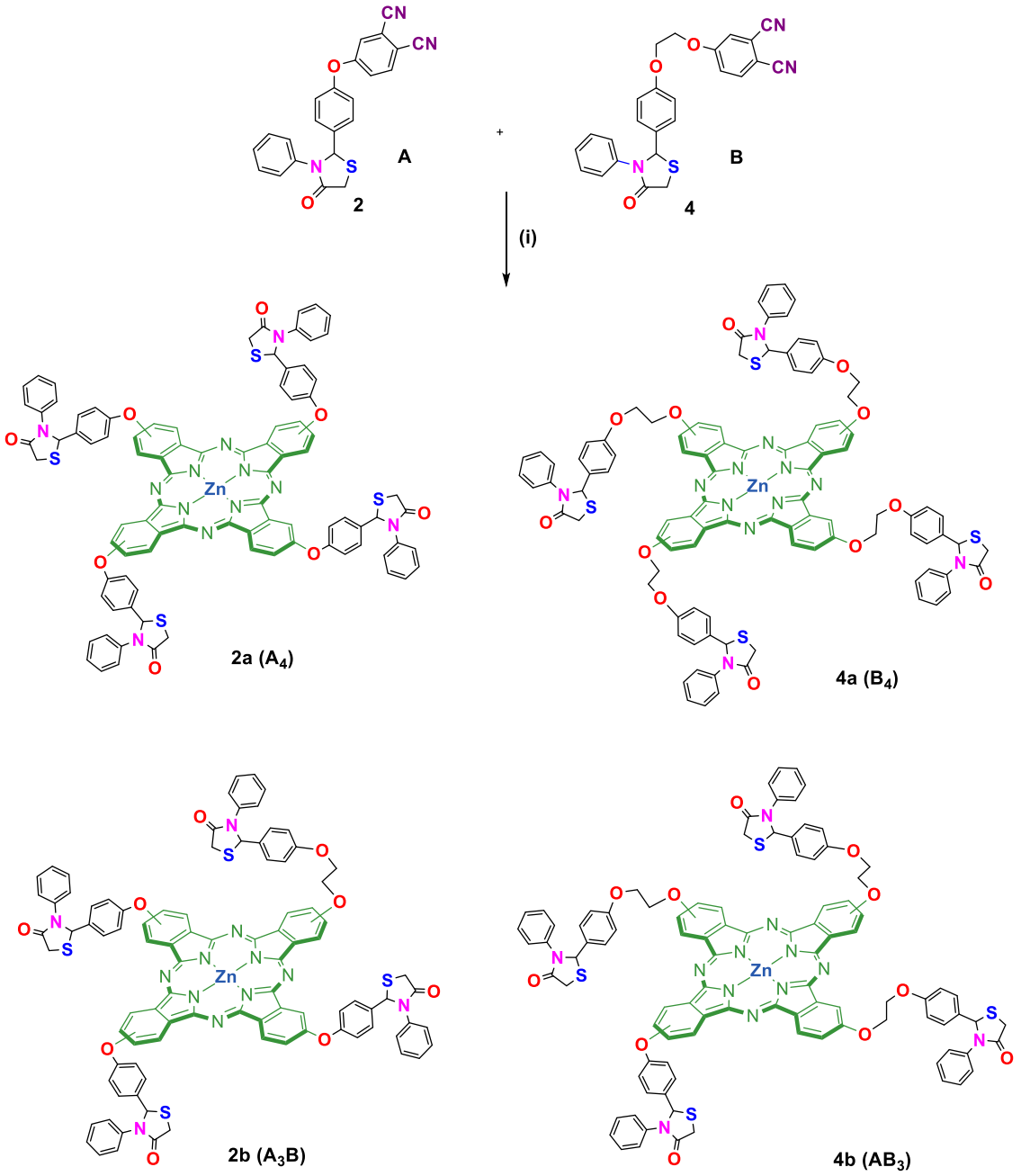

Scheme 2. Synthesis of symmetrical ZnPcs (2a, 4a) and unsymmetrical ZnPcs (2b, 4b). (i) DMF, DBU, $Zn(OAc)_2{\cdot}2H_2O$, 24 h, 160 °C.

Fig. S14, and Fig.S16 for 2, 4, 2a, 2b, 4a, and 4b, respectively. The IR spectrum of the 4-(4-(4-oxo-3-phenylthiazolidin-2-yl)phenoxy)phthalonitrile (2) exhibited vibrations of aromatic (Ar-H) peak at 3046–3077 cm^{-1} and (C≡N) group peak at 2232 cm^{-1}, while the stretching vibration of (C = O) group peak was determined at 1682 cm^{-1}.Similarly, with the IR spectra of 4-(2-(4-(4-oxo-3-phenylthiazolidin-2-yl)phenoxy)ethoxy)phthalonitrile (4), peaks were observed at 2925 cm^{-1} for aromatic (Ar-H), at 2231 cm^{-1} for C = N stretching, and at 1677 cm^{-1} for (C = O) stretching frequencies, respectively. It was seen that the OH bands both at 3095 cm^{-1} for compound 1 and 3356 cm^{-1} for compound 3 disappeared in all spectra after phthalonitrile formation. In addition, the formation of new metallophthalocyanines (2a, 2b, 4a, and 4b) from compounds 2 and 4 as in Scheme 2 was accomplished by the disappearance of the –C = N vibration at 2232 cm^{-1} and 2231 cm^{-1}, respectively. This proved that cyclotetramerization had taken place successfully.

When the proton NMR of the compounds (2, 3, 4) before cyclotetramerization was examined, resonance frequencies between 6 and 4.5–3.9 ppm were observed for all specific protons ($H_{methylenic}$ protons and $H_{quaternary}$proton between N and S in the thiazolidon, respectively) (Fig.1). Regarding the other characteristic protons, when compound 1 turned to compound 3 by the addition of ethanediol, the four protons belonging to the ethylene group in the aliphatic chain for compound 3 resonated as multiplets between 4.28 and 3.93 ppm. When the hydroxyl groups in compounds 1 and 3 were masked by phthalonitrile, the most characteristic proton (Ha) adjacent to the nitrile ring in the resulting compounds 2 and 4 resonated at 7.72 ppm with an interaction as a doublet (J = 8.5 Hz). Likewise, the methylenic protons for com-

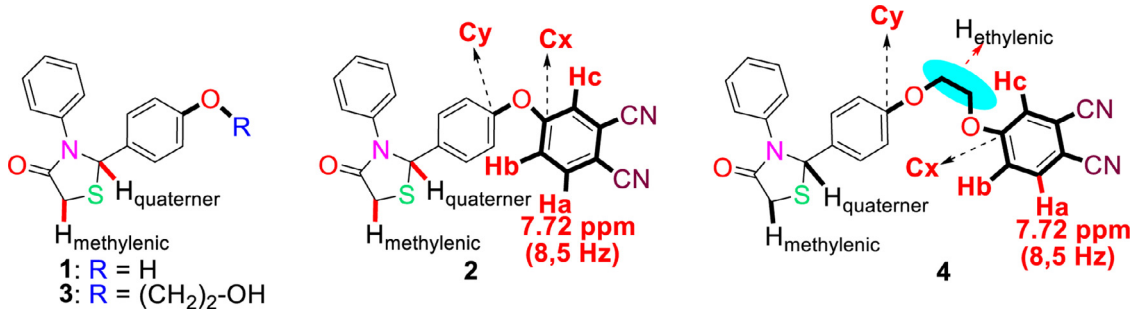

Fig. 1. Synthesis compounds 1–4.

pound 4 were resonated as multiplets at 4.37 and 4.44 ppm, respectively.

In the ^{13}C NMR spectrum, all the ethylenic, methylenic, quaternary, and carbonyl carbon signals of compounds 2, 3, and 4 were resonated at the deserved region. The resonated signals were 171.1 (C = O), 65.1 (-CH=), and 33.7 (-CH_2-) for compound 2; 171.5 (C = O), 69.5 (-CH_2-), 65.6 (-CH=), 61.1 (-CH_2-), and 33.9 (-CH_2-) for compound 3; and 171.6 (C = O), 69.5 (-CH_2-), 65.6 (-CH_2-), 61.1 (-CH=), and 33.9 (-CH_2-) for compound 4. Other distinguishing carbons for compounds 2, 3, and 4 were the resonance frequencies of carbons (marked by Cx, Cy) bonded to oxygen. These marked carbons (Cx, Cy) resonated at 161.4, 154.2 ppm for compound 2, 159.3, 137.6 ppm for compound 3, and 162.0, 158.7 ppm for compound 4, respectively. Regarding the resonance signals of the aromatic ring carbons of compounds 2, 3, and 4, it was impossible to see all of them in different regions since some of the carbons overlapped as a result of resonating in the same region. Although tetrasubstituted metallophthalocyanine complexes with positional isomers dissolve in many organic solvents, their ^1H- and ^{13}C NMR spectra could not be obtained, possibly due to dynamic NMR stability, the bulky group effect, and aggregation tendencies.

The MALDI-TOF mass spectra of phthalocyanines were also recorded; as: *m/z* $[M]^+$calcd. for $C_{92}H_{60}N_{12}O_8S_4Zn$:1652.28, found: [$M^+$] 1652.53 for 2a.; as: *m/z* $[M]^+$calcd. for $C_{94}H_{64}N_{12}O_9S_4Zn$: 1699.24, found: [$M^+$] 1700.04. for 2b.; as: *m/z* $[M]^+$calcd. for $C_{100}H_{76}N_{12}O_{12}S_4Zn$: 1831.40, found: [$M^+$] 1831.43. for 4a.; as: *m/z* $[M]^+$calcd. for $C_{98}H_{72}N_{12}O_{11}S_4Zn$: 1784.36; found: [$M+$] 1787.88. for 4b, respectively.

3.2. UV–Vis absorption spectra and aggregation behavior

Phthalocyanines are generally given two absorption bands (Q and B) at approximately 670 nm and 300 nm, respectively [59]. The Q bands of the synthesized phthalocyanine compounds were observed at about 680–683 nm, and the B bands were observed at about 356–360 nm. Peripherally symmetrical 2a and 2b and unsymmetrical 4a and 4b zinc(II) phthalocyanine complexes were synthesized and UV–Vis absorption properties were analyzed. All synthesized phthalocyanines were dissolved in common organic solvents such as THF, DCM, $CHCl_3$, DMSO, and DMF (Fig. 2, Fig. S17).

Aggregation (such as low solubility and the prevention of optical and electrochemical properties) is the most important problem. It prevents the interaction of phthalocyanines in various applications, such as in photodynamic therapy [60]. The solubility and aggregation tendencies of symmetric (**2a, 4a**) and unsymmetrical (**2b, 4b**) compounds in DMF were investigated (Fig. 3).

Whereas compound **4a** (Fig.S17) showed mild aggregation, compounds **2a, 2b,** and **4b** did not show any aggregation behavior in different solvents at a concentration of 1×10^{-5} M. as shown in Fig. 3. The UV–Vis spectra exhibited the typical shape of Pcs

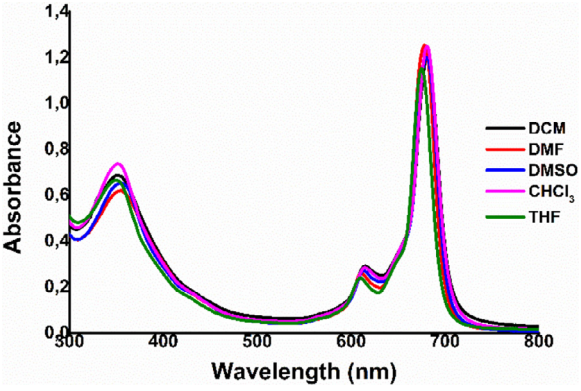

Fig. 2. UV–Vis absorption spectra of compound (2a) in different solvents at 1.00×10^{-5} M.

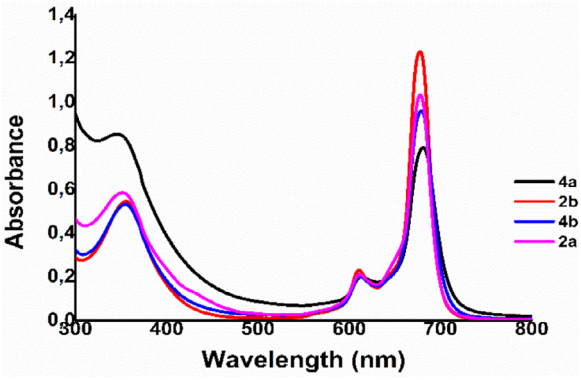

Fig. 3. UV–Vis spectra of symmetrical (2a, 4a) and unsymmetrical (2b, 4b) ZnPcs in DMF at a concentration of 1×10^{-6} M.

with an intense sharp Q band at around 680–683 nm for all the synthesized zinc-containing complexes (**2a, 2b, 4a, 4b**) in DMF. As a result, both symmetrical and unsymmetrical phthalocyanine compounds showed the highest absorption in DMF. Therefore, in the photophysical and photochemical studies, aggregation properties were examined in the same solvent at different concentrations (Fig. 4). The concentration effect on the aggregation properties of the **2a, 2b, 4a**, and **4b** compounds were also studied at various concentrations ranging from 2×10^{-6} to 1.2×10^{-5} M in DMF.

It was observed that not all compounds agglomerated in this working range, as no blue shift (shorter wavelength shift) was observed in absorption against concentrations of 10^{-6}–10^{-5} M. In addition, the results obtained from the UV–Vis graphs in the Q band (maximum wavelength) show that the ratio between concentration and absorption at the time of plotting changed according to the Lambert–Beer law. The spectroscopic properties and aggrega-

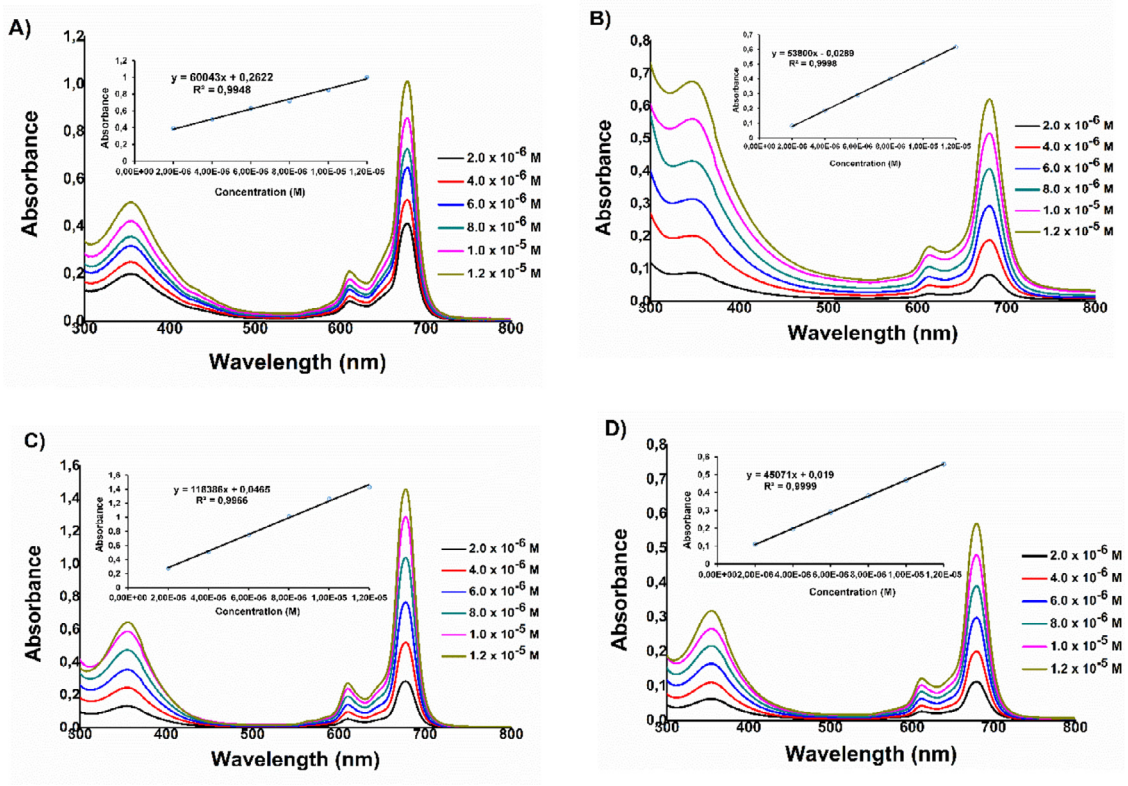

Fig. 4. UV–Vis spectra of symmetrical (A–B) and unsymmetrical (C–D) ZnPcs in different concentrations (in DMF): (A) 2a, (B) 4a, (C) 2b, and (D) 4b.

Table 1
Absorption, excitation and emission spectral data for **2a, 2b, 4a**, and **4b** standard studied ZnPc (in DMF).

Compound	Q band λ_{max}(nm)	log ε	Excitation λ_{Ex}, (nm)	Emission λ_{Em}, (nm)	Stokes shift (nm)
2a	680	4.09	678	690	12
2b	683	4.89	–	–	
4a	681	4.70	682	692	10
4b	682	4.97	684	690	6
ZnPc[a]	670	5.37	670	676	6

[a] Data from Zorlu et al. (2010) [64].

Table 2
Photophysical, photochemical and fluorescence quenching parameters of ZnPcs (**2a, 2b, 4a**, and **4b**) in DMF.

Compounds	Φ_F	Φ_Δ	Φ_d (x10^{-4})	Ksv (M^{-1})
2a	0.09	0.78	0.74	32.9
2b	–	0.24	0.40	27.3
4a	0.16	0.04	0.38	24.2
4b	0.11	0.08	0.45	29.8
ZnPc[a]	0.17	0.56	0.23	57.60[b]

[a] Data from Zorlu et al. (2010) [62] and Spiller et al. (1998) [67].
[b] Data from Gurol et al. (2007) [71].

tion behavior were evaluated in DMF; the results are summarized in Table 1 and Table 2.

3.3. Photophysical properties

3.3.1. Evaluation and interpretation of fluorescence spectra

The absorption, emission, and excitation spectra of the ZnPc complexes (2a, 2b, 4a, 4b) are shown in Fig. 5 (using complex 2a, as an example) and Fig. S18, and the data are summarized in Table 1. While zinc(II) phthalocyanine derivatives (2a, 4a, and 4b) showed fluorescence emission and excitation, compound 2b did not give any fluorescence emission signal. This is thought to be due to the effect of substituent groups attached to the ZnPc ring.

The Stokes shift values (Δ_{Stokes}) of substituted zinc(II) phthalocyanines (2a, 4a, 4b) were found to be 12, 10, and 6 nm, respectively. In addition, the Stokes value of complex 4b (6 nm) was found to be similar to Std-ZnPc. As can be seen in Fig. 5, the excitation and absorption spectra of complex 2a were similar. This shows that the nuclear configurations of the ground and excited states were similar and not affected by excitation in DMF [18,61].

3.3.2. Fluorescence quantum yields (Φ_F)

The fluorescence quantum yields (Φ_F) of all compounds (2a, 2b, 4a, and 4b) were determined in DMF using the methods described in the literature [62]. Compounds 2a, 4a, and 4b showed medium fluorescence emission, while compound 2b could not be studied due to the absence of fluorescence emission [60]. The yields were also calculated for the zinc(II) phthalocyanine compounds (2a, 2b, 4a and 4b). The results are listed in Table 2. The Φ_F values of the ZnPc compounds (2a, 2b, 4a, and 4b), compared with standard ZnPc (0.17) in DMF, were lower. However, the fluorescence quantum yield (0.16) of compound 4a was found to be close to that of standard ZnPc (0.17).

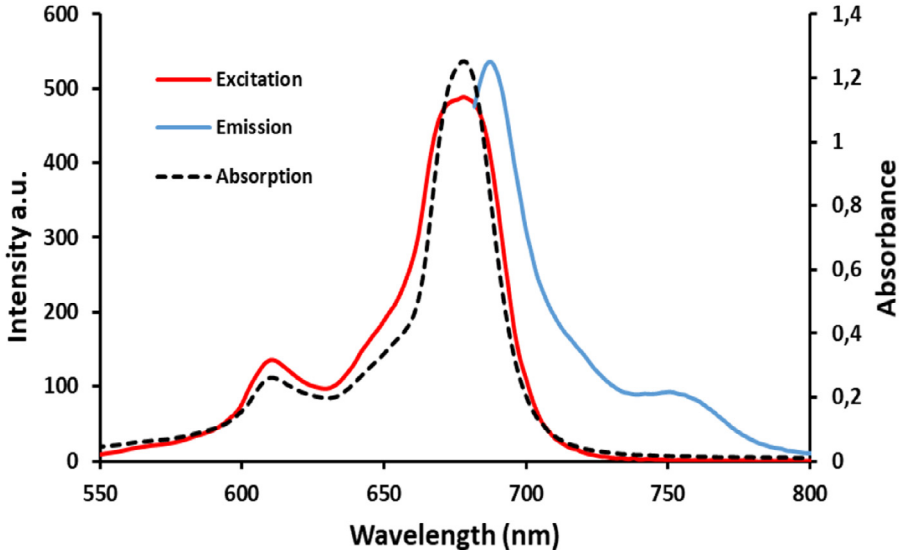

Fig. 5. UV–Vis absorption (black dashedlines), excitation (red solidlines), andemission (navy solidline) spectra of the symmetrical Pc complex (2a) in DMF.

3.4. Photochemical studies

3.4.1. Singlet oxygen quantum yield (Φ_Δ)

An ideal photosensitizer, which has an important place in photodynamic therapy, is determined by its phototoxic singlet oxygen capability. Singlet oxygen is produced when oxygen in the triple ground state interacts with a photosensitizer. This is known as photosensitization. The proportion of singlet oxygen supplied by the excited phthalocyanine can be expressed by singlet oxygen quantum efficiency (Φ_Δ) [63]. Singlet oxygen quantum efficiency (Φ_Δ) determinations were performed according to the experimental setup in the literature [54]. 1,3-Diphenylisobenzofuran (DPBF) was used as a chemical quencher for singlet oxygen in DMF. Disappearance at the DPBF peak was spectroscopically monitored by sending light to the solution (at 417 nm). There was no significant change in the intensity of the Q band during the experiment. This shows that phthalocyanines are not degraded during singlet oxygen measurement [64,65]. It is known that the singlet oxygen quantum yield depends on the triplet quantum yield of the photodetector, and complexes with high triplet quantum yields are expected to have high singlet oxygen quantum yields [66]. The singlet oxygen quantum efficiencies of the ZnPcs (2a, 2b, 4a and 4b) (Φ_Δ) were calculated via Eq. (1) using standard ZnPc (Φ_Δ=0.56 in DMF) [62,67].

$$\Phi_\Delta = \Phi_\Delta^{Std} \frac{R \cdot I_{abs}^{Std}}{R^{Std} \cdot I_{abs}}, \quad (1)$$

where $\boldsymbol{\Phi_\Delta^{Std}}$ is the singlet oxygen quantum yields for the standard ZnPc ($\boldsymbol{\Phi_\Delta^{Std}}$ = 0.56 in DMF) [62,67]. $\boldsymbol{R}$ and $\boldsymbol{R^{std}}$ are the DPBF photobleaching rates in the presence of the respective samples (2a, 2b, 4a, and 4b) and standard, respectively. I_{abs} and $\mathbf{I_{abs}^{Std}}$ are the rates of light absorption by the samples (2a, 2b, 4a, and 4b) and standard, respectively. The light intensity 8.15 × 10^{15} photons s^{-1} cm^{-2} was used for Φ_Δ determinations.

Following the calculations, singlet oxygen quantum efficiencies Φ_Δ values were recorded as 0.78, 0.24, 0.04, and 0.08for ZnPcs 2a, 2b, 4a, and 4b, respectively (Fig. 6, Table 2). As can be seen from Table 2, the singlet oxygen quantum yield (Φ_Δ) of complex 2a was higher than that of other phthalocyanine complexes (2b, 4a, and 4b). 2a also showed a higher singlet oxygen quantum yield (Φ_Δ = 0.78) than containing thiazole groups ZnPc derivatives (Φ_Δ = 0.61 for lit. [68]), Φ_Δ = 0.62 for lit [69]., and Φ_Δ = 0.71 for lit [70]. in DMF). It is thought that the substituted groups [69b], attached to the phthalocyanine ring played an important role changing the efficiency of singlet oxygen formation by the bulky group effect [9]. Additionally, compared to the standard ZnPc, it can be said that the high singlet oxygen generation of compound 2a was quite satisfactory in terms of its potential use in PDT as a photosensitizer.

3.4.2. Photodegradation and quantum yield (Φ_d)

Photodegradation quantum yield (Φ_d) determinations were conducted using the experimental setup described in the literature [54,72,73] Determination of the stability of phthalocyanine derivatives under light irritation is very important for molecules designed to be used in PDT. An ideal photosensitizer should spend enough time in the body without disrupting and should be removed from the body after completing activation at the optimal time [74]. The targeted photostabilities were determined by reducing the absorption spectra of the zinc(II) phthalocyanines (2a, 2b, 4a, and 4b) measured under light illumination in DMF at a concentration of 1 × 10^{-5} M (Fig.7). The reduction of the Q bands of symmetric and unsymmetrical phthalocyanine complexes was monitored by UV–Vis, and spectroscopy was defined by the photodegradation quantum yield (Φ_d). A light intensity of 3.26 × 10^{16} photons s^{-1} cm^{-2} was employed for Φ_d determinations. Photodegradation quantum efficiencies were determined according to Eq. (2). The calculated Φ_d values are given in Table 2.

$$\Phi_d = \frac{(C_0 - C_t) \cdot V \cdot N_A}{I_{abs} \cdot S \cdot t}, \quad (2)$$

where C_0 and C_t are the concentrations of the samples before and after irradiation, respectively. V is the reaction volume, N_A is the Avogadro constant, S is the irradiated cell area, t is the irradiation time, and I_{abs} is the overlap integral of the radiation source light intensity and the absorption of the samples [54,63].

Based on the data in Table 2, the photodegradation quantum yields of all synthesized phthalocyanine complexes (2a, 2b, 4a, 4b) appear to have had roughly similar stability (with the exception of 2a). It is known that phthalocyanine complexes used in PDT are considered stable with values as low as 10^{-6} and unstable with values around 10^{-3} [74]. Accordingly, we can say that the synthesized ZnPc complexes had intermediate photostability. When photodegradation quantum yields (Φ_d) are compared with standard ZnPc, it can be seen that both symmetric (2a, 4a), and unsymmetric (2b, 4b) phthalocyanine complexes had lower photostability.

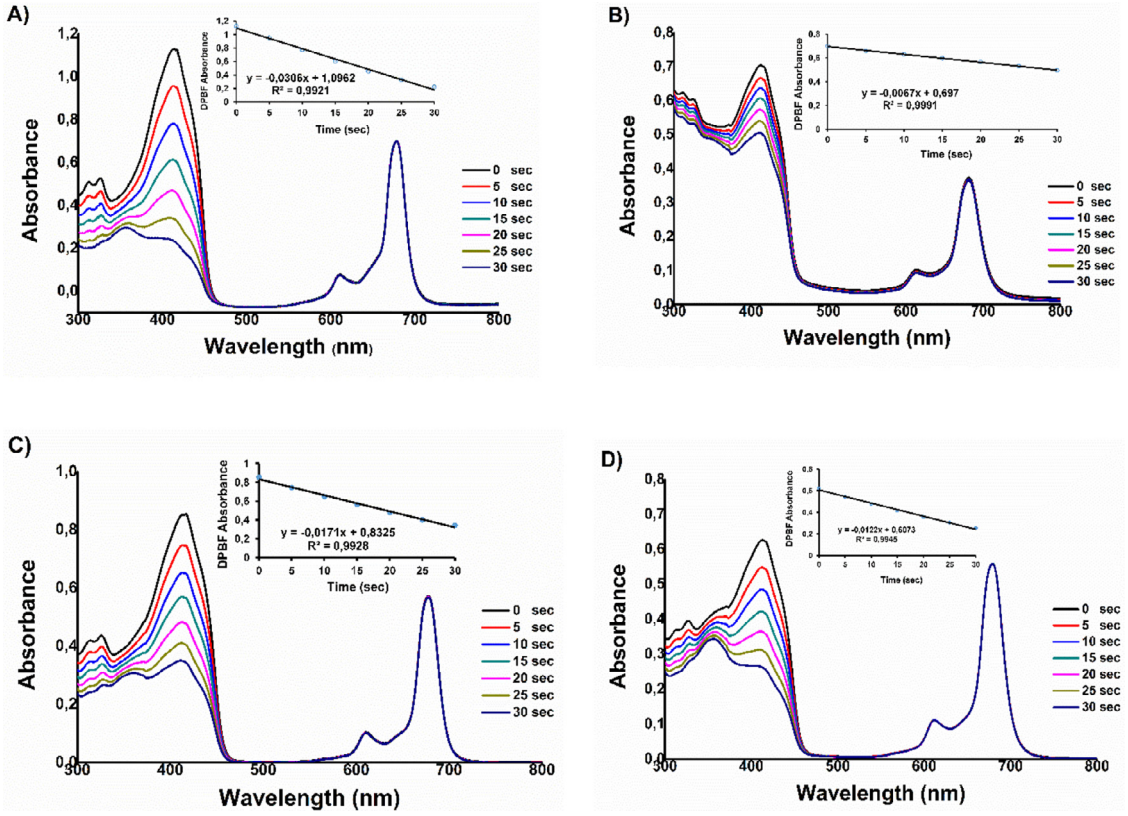

Fig. 6. Singlet oxygen UV–Vis spectra with DPBF at different times of symmetrical (**2a, 4a**) and unsymmetrical (**2b, 4b**) Pc complexes: (A) **2a**, (B) **4a**, (C) **2b**, and (D) **4b** in DMF at a concentration of 1×10^{-5} M.

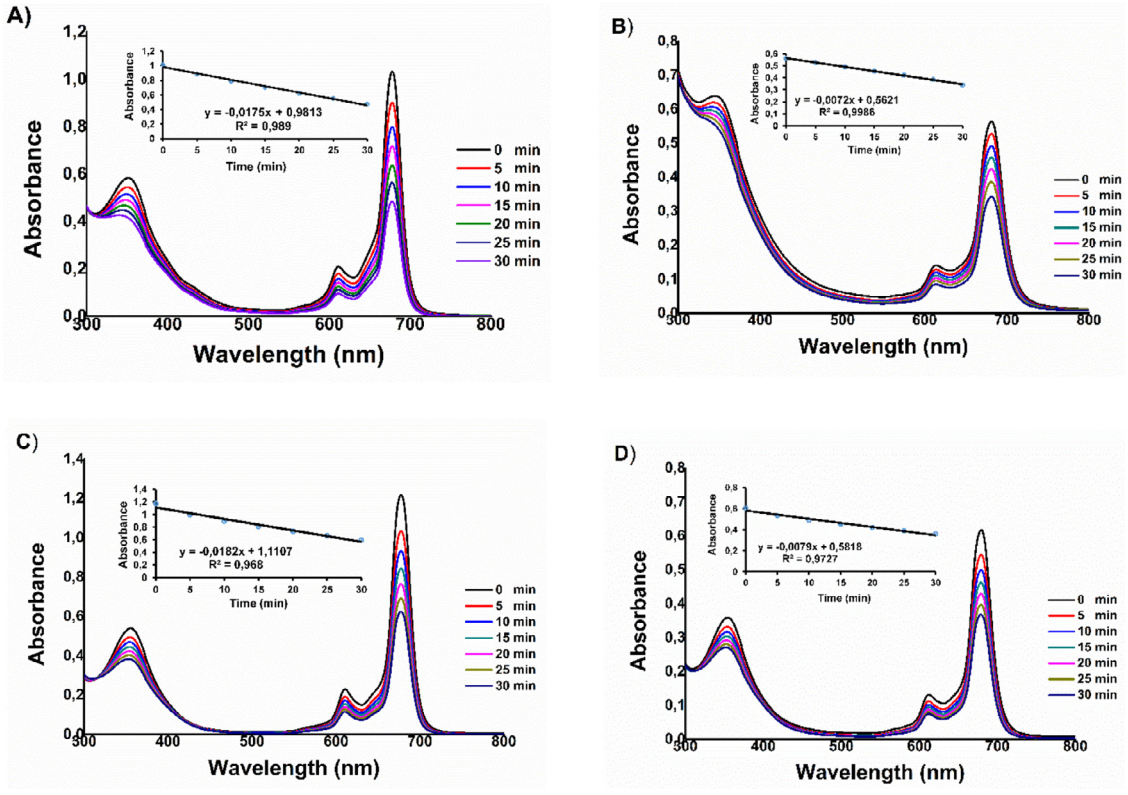

Fig. 7. Photodegradation of symmetrical (**2a, 4a**) and unsymmetrical (**2b, 4b**) Pc complexes (A) **2a**, (B) **4a**, (C) **2b**, and (D) **4b** in DMF at a concentration of 1×10^{-5} M showing the disappearance of the Q band at 5 min intervals (inset: plot of Q band absorbance versus time).

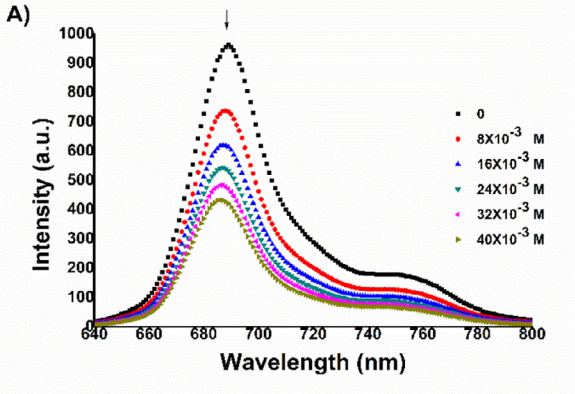

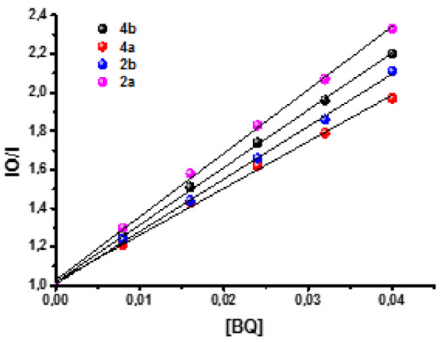

Fig. 8. (A) Fluorescence emission spectral changes of 2a (1.00×10^{-5} M) on addition of different concentrations of BQ in DMF. (B) S–V plots for BQ quenching of substituted ZnPc complexes 2a, 2b, 4a, and 4b in DMF.

From the literature, it can be noted that substituted groups of phthalocyanines containing chemically active sites are high, while the photodegradation value of zinc(II) phthalocyanine complexes carrying chemically stable substituents is low [75,76,9a]. Thus, it can be said that the zinc(II) phthalocyanine complexes (2a, 2b, 4a, 4b) that have chemically substituents compared to the previously synthesized phthalocyanines are stable.

3.5. Fluorescence quenching studies by 1,4-benzoquinone [BQ]

Fluorescent quenching experiments were performed on symmetric (2a, 4a) and unsymmetric (2b, 4b) ZnPc derivatives (in DMF) [54]. These were accomplished by adding BQ concentrations (0, 0.008, 0.016, 0.024, 0.032, and 0.040 M) to a fixed concentration of complexes (Fig. 8A). Here, suitability to Stern–Volmer (S–V) kinetics was examined. By adding 1,4-BQ (quencher), energy transfer between fluorophore (the excited ZnPc) and the quencher occurred. The S–V constants (Ksv) of the studied zinc(II) phthalocyanines (2a, 2b, 4a, 4b) are shown in Table 2. The quenching spectra of fluorescence intensity related to the BQ concentration of synthesis complexes can be seen in Fig. 8A and Fig. S19. From Fig. 8B, it can be seen from the linearity in the slope graph of the plots that the diffusion-controlled quenching mechanism occurred as expected. The fluorescence spectra of symmetrical (2a, 4a) and unsymmetrical (2b, 4b) zinc(II) phthalocyanines BQ concentrations were recorded, and the changes in fluorescence intensity related to BQ concentration by the S–V equation [77] can be seen in Eq. (3):

$$I_0/I = 1 + Ksv[BQ]. \quad (3)$$

Where I_0 and I are the fluorescence intensities of fluorophore in the absence and presence of quencher, respectively. BQ is the concentration of the quencher, and Ksv is the S–V constant.

In this study, it was thought that there might be a ground state interaction between synthesis complexes and BQ since no shifts in different peaks and wavelengths could be observed. The Ksv values of the phthalocyanines studied (32.9, 27.3, 24.2, and 29.8 M^{-1} for compounds 2a, 2b, 4a, and 4b, respectively) in DMF were found to be low compared to the standard unsubstituted ZnPc (57.60 M^{-1}). This suggests that the substitution of the phthalocyanine ring reduced the Ksv value (Table 2) [63].

3.6. Electrochemical studies for ZnPc compounds

Cyclic voltammetry (CV) was used to investigate the electrochemical properties of 2a, 2b, 4a, and 4b (Figs. 9-10 and Fig. S20). Cyclic voltammograms of the ZnPc compounds (Dyes) were recorded using Gamry Interphase 1000 Potentiostat with their

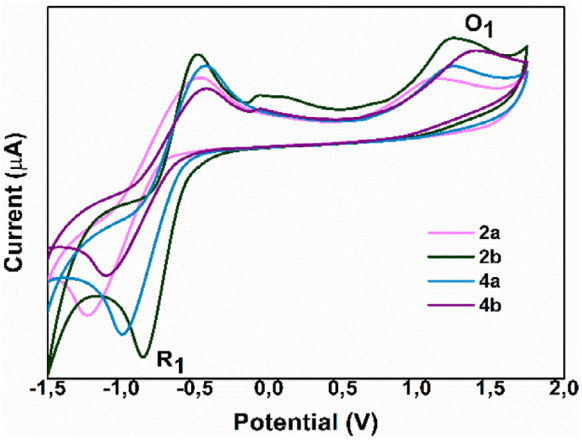

Fig. 9. Cyclic voltammograms of complexes **2a, 2b, 4a**, and **4b** in DMF containing 0.1 M $TBAPF_6$ (scan rate = 100 mVs^{-1}).

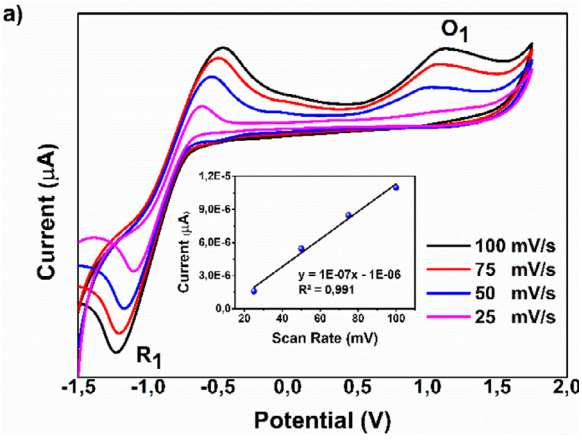

Fig. 10. Cyclic voltammograms of complex 2a in DMF containing 0.1 M $TBAPF_6$ (scan rate from 25 to 100 mVs^{-1}).

electrode system; glassy carbon served as the working electrode, Pt disk as the reference electrode, and Pt wire as the counter electrode at a scan rate of 100 mV/s. All electrochemical measurements were conducted in DMF solvent containing tetrabutylammonium hexafluorophosphate ($TBAPF_6$) as the supporting electrode, and Fc/Fc^+ redox couple was utilized as the external standard to calibrate the results. Cyclic voltammograms of the complexes cali-

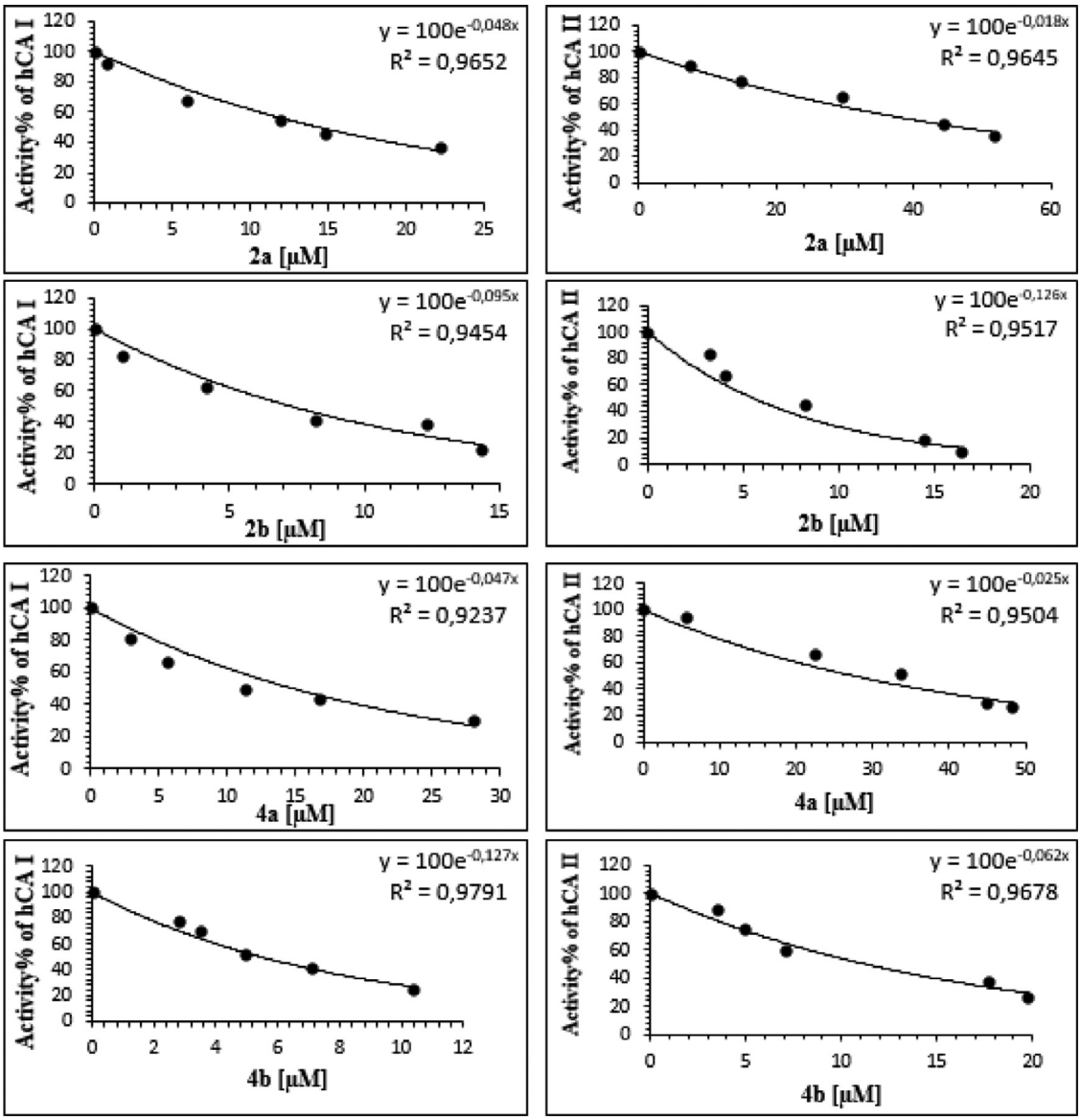

Fig. 11. IC_{50} graphs of 2a, 2b, 4a, and 4b for hCA I and II.

Table 3
Electrochemical properties of **2a, 2b, 4a** and **4b.**

Dye	λ_{max} (nm)	λ_{onset} (nm)	$E_{o\text{-}o}$ (eV)[a]	E_{red} (V)	E_{ox} (V)	$E_{HOMO/LUMO}$ (eV) [b,c]
2a	680	699	1.77	−1.07	0.67	−5.11 / −3.34
2b	683	700	1.77	−0.79	0.86	−5.30 / −3.53
4a	681	697	1.78	−0.91	0.75	−5.19 / −3.41
4b	682	703	1.76	−0.92	0.78	−5.22 / −3.46

[a] Band gap ($E_{0\text{-}0}$) was calculated from the absorption onset wavelength (λ_{onset}) using $E_{0\text{-}0} = 1240/\lambda_{onset}$.
[b] HOMO level was calculated by the equation HOMO = -(4.8 + $E_{1/2}$) (vs. Fc/Fc^+) [78]. In this equation, 4.8 eV is the energy level of ferrocene/ferrocenium couple below the vacuum level.
[c] LUMO level was estimated from $E_{LUMO=}$ E_{HOMO} + $E_{0\text{-}0}$. [79].

brated with external ferrocene standard (0.36 V vs Pt disk pseudo-reference electrode) and recorded at 100 mV/s can be seen in Fig. 9. The electrochemical parameters can be seen in Table 3. In the study, a nitrogen atmosphere was maintained throughout the cyclic voltammogram scans from 25 to 100 mV/s (Fig. 10 and Fig. S20).

In this study, a high current intensity anodic peak was obtained without the appearance of any cathodic peak, showing that both symmetrical and unsymmetrical phthalocyanines were irreversibly oxidized (Fig. 9 and Fig. S20) [80]. As shown in Fig. 9, the ZnPc compounds (2a, 2b, 4a, 4b) gave phthalocyanine ring-based reversible reduction peaks at −1.07 V, −0.79 V, −0.91 V, and −0.92 V in addition to the irreversible oxidation peaks at 0.67 V, 0.86 V, 0.75 V, and 0.78 V, respectively. It is well known that the central metal ion can reduce or oxide when the d-orbitals of the metal ion locate between the HOMO and LUMO of the ring [81].

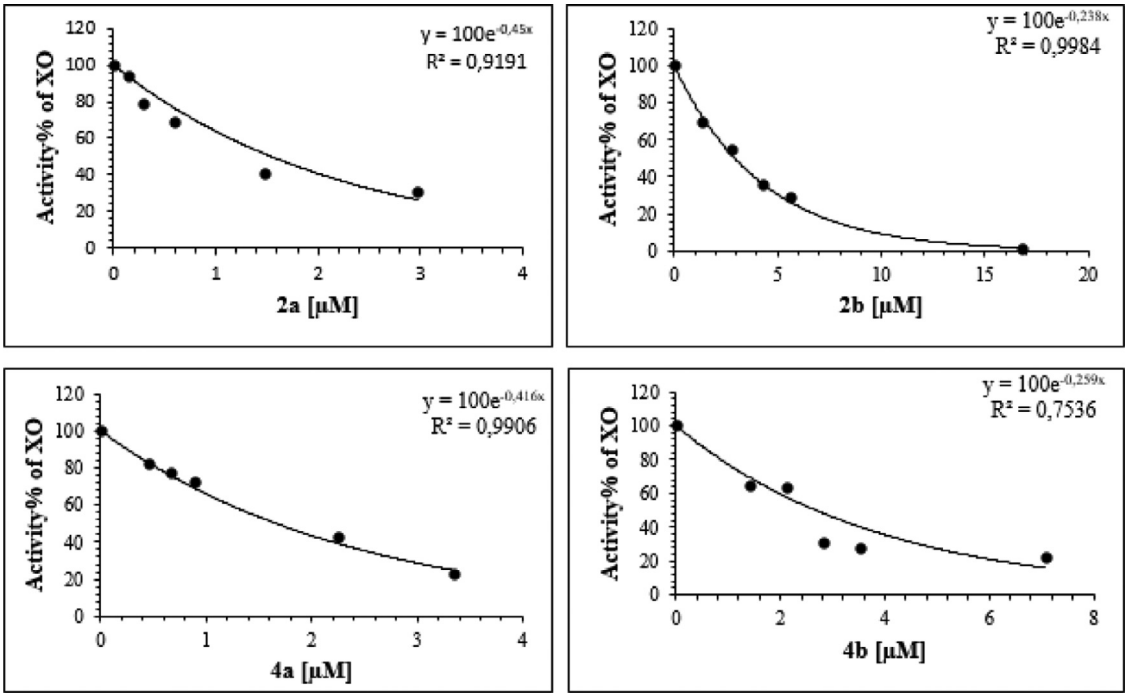

Fig. 12. IC_{50} graphs of 2a, 2b, 4a, 4b for XO.

For all ZnPc compounds, it can be seen from Table 3 that HOMO energies were between −5.11 and −5.30, while LUMO energies were between −3.34 and −3.53 Fig. 10. and Fig. S20 show that the reversibility of the oxidative process remained almost unchanged with different scan rates for complexes 2a, 2b, 4a, and 4b; thus, it can be said that dye ZnPc showed good redox stability. The peak currents of the R_1 and O_1 processes increased linearly with the square root of the scan rate, indicating their diffusion-controlled structure [82].

3.7. Enzyme inhibition results

As CA isoenzymes are involved in many vital physiological functions, inhibitors of these isoenzymes have found a place in clinical applications to treat many diseases, ranging from glaucoma to epilepsy and even cancer. However, identifying new, effective, isoenzyme-specific inhibitors has been the target of biomedical studies due to the non-specificity of CA inhibitors (AZA, brinzolamide, dorzolamide, etc.) used in clinical practice and their various side effects [22,24]. XO inhibitors are target molecules that can be used in the treatment of uric acid accumulation in the body and hyperuricemia caused by superoxide anion radicals and other related diseases [35,36]. Allopurinol, febuxostat, and to piroxostat, which are approved as XO inhibitors in clinical use, have severe adverse effects [36]. Therefore, the identification of new, potent XO inhibitors with fewer side effects is an urgent requirement. In a few previous studies, the inhibition effects of synthesized phthalocyanines on CA [11,15], and XO [12,15,47] activity were determined. Given the importance of CA and XO inhibitors in light of this information, we investigated the inhibition effects of zinc(II) phthalocyanines containing thiazolidin-4-one that we synthesized in this study on hCA I, hCA II, and XO activities.

The inhibition effects of thiazolidin-4-one containing zinc(II) phthalocyanines and ligands (1 and 3) on hCA I and II activities are presented in Table 4. The inhibition effects of ligands (1 and 3) and phthalocyanines synthesized (2a, 2b, 4a, 4b) in this study on hCAI and II isoenzymes were determined using IC_{50} values. AZA was used as the reference inhibitor for both isoenzymes. It was

Table 4
Inhibition results of thiazolidin-4-one containing zinc(II) phthalocyanines and ligands on hCA I and hCA II isoenzymes.

Compounds	IC_{50} for hCA I	R^2	IC_{50} for hCA II	R^2
1	8.54 µM	0.9309	5.22 µM	0.9679
3	5.64 µM	0.9259	4.86 µM	0.9771
2a	14.58 µM	0.9652	38.8 µM	0.9645
2b	7.36 µM	0.9454	5.55 µM	0.9517
4a	14.89 µM	0.9237	28 µM	0.9504
4b	5.51 µM	0.9791	11.29 µM	0.9678
AZA	0.643 µM	0.9344	0.457 µM	0.9890

*Acetazolamide (AZA) used as a standard inhibitor for hCA I and hCA II isoenzymes.

observed that **4b** was the most potent hCA I inhibitor, while **4a** had the weakest inhibitory effect on hCA I. Regarding hCA I, the inhibitors can be ranked as follows: **4b**>**2b**>**2a**>**4a**. In contrast, **2b** had the strongest inhibitory effect on hCA II, while **2a** showed the weakest inhibitory effect. Regarding hCA II, the inhibitors can be ranked as follows: **2b**>**4b**>**4a**>**2a**. Although the inhibition effects of **2a, 2b, 4a**, and **4b** were at micromolar levels in the case of hCA I and II isoenzymes, it was observed that these molecules exhibited a weaker inhibitory effect than AZA in this respect. The IC_{50} values of **2a, 4a, 2b, 4b** and AZA in relation to hCA I and II are given comparatively in Fig. 11. In addition, when the inhibition effects of the synthesized molecules for hCA I and II were compared with the starting compounds **1** and **3**, it was observed that **4b** had a stronger inhibition effect against hCA I than the ligands (**1** and **3**). In terms of hCA I inhibition, **2b** had a stronger inhibition effect than ligand **1** but was less effective than ligand **3**. The **2a** and **4a** molecules showed weaker inhibition effects on hCA I activity than **1** and **3**, while starting compounds **1** and **3** exhibited stronger inhibition effects on hCA II activity than **2a, 4a, 2b**, and **4b**.

The activities of thiazolidin-4-one containing zinc(II) phthalocyanines and ligands (1 and 3) against XO were tested. The results of this testing can be seen in Table 5, IC_{50} values were determined by calculating the results obtained in these activity tests. Allopurinol was used as a reference inhibitor against XO. From the results,

Table 5
Inhibition results of thiazolidin-4-one containing zinc(II) phthalocyanines and ligands (**1** and **3**) on XO.

Compounds	IC_{50} for XO	R^2
1	No inhibition effect	–
3	No inhibition effect	–
2a	1.54 μM	0.9191
2b	2.91 μM	0.9984
4a	1.67 μM	0.9906
4b	2.60 μM	0.7536
Allopurinol*	20 μM	0.9578

* Allopurinol used as a standard inhibitor for XO.

it appears that 2a was the most potent XO inhibitor, while 2b had the least potent XO inhibitory effect (Fig.12). It can also be seen that 2a, 2b, 4a, and 4b had a much stronger inhibitory effect on XO than on hCA I and II isoenzymes. Starting compounds 1 and 3, in contrast, had no significant inhibition effect on XO activity.

4. Conclusion

In this study, we reported on the synthesis of novel symmetrical and unsymmetrical phthalocyanine compounds that were characterized using spectrometry (FTIR, UV–Vis, MALDI-TOF mass) and NMR spectroscopy. The photochemical behavior of the complexes was studied. Photophysical and photochemical analyses of synthesized ZnPc compounds was performed in DMF. Considering the quantum yields, it can be determined that complex 2a had the highest singlet oxygen quantum efficiency (0.78), whereas complex 4a had the lowest quantum efficiency (Table 2). This is thought to be due to bulky groups influence and the substituted groups effect on the phthalocyanine. In addition, complex 2a had higher quantum efficiency (Φ_Δ) compared to Std-ZnPc. It can be said that compound 2a is quite satisfactory for potential use in PDT as a high singlet oxygen generation photosensitizer. It was also discovered that the newly synthesized phthalocyanines (2a, 2b, 4a, 4b) had potent inhibitory effects on hCA isoenzymes (I and II) and XO. At very low micromolar concentrations, these molecules inhibited hCA I, hCA II, and XO enzymes. The inhibitory effects on XO enzyme activity were more potent. 2b (for hCA I IC_{50}: 7.36 μM, for hCA II IC_{50}: 5.55 μM) and 4b (for hCA I IC_{50}: 5.51 μM, for hCA II IC_{50}: 11.29 μM) showed stronger inhibition effects against hCA I and II than 2a (for hCA I IC_{50}: 14.58 μM, for hCA II IC_{50}: 38.8 μM) and 4a (for hCA I IC_{50}: 14.89 μM, for hCA II IC_{50}: 28 μM). Although the inhibition effects of these molecules were similar for the XO enzyme, 2a (IC_{50}: 1.54 μM) was the most potent. These results may assist in the development of new CA and XO inhibitors investigated in drug design studies for clinical applications.

Credit authorship contribution statement

Arif Baran: Methodology, Investigation, Conceptualization, analysis, data curation, writing-original draft. Emel Karakılıç: Synthesis, analysis, photophysics, and photo-chemical experiment, electrochemical experiment. Zuhal Alım and Aslıhan Günel: Biological investigation.

Declaration of Competing Interest

The authors declare that there is no conflict of interest.

Acknowledgment

This work is financially supported by the (TÜBITAK, Project no: 115Z446 and 217Z043) and the Scientific Research Projects Department (BAP) of Sakarya University Organic Chemistry Laboratory (Project no: 2021–7-25–2).

Supplementary materials

Supplementary material associated with this article can be found, in the online version, at doi:10.1016/j.molstruc.2022.132630.

References

[1] C.C. Leznoff, & A.B.P. Lever, Properties and Applications VCH, New York 1996 (1989).
[2] J.H. Zagal, F. Bedioui, J.P. Dodelet, N4-macrocycle Metal Complexes, Springer, New York, 2006.
[3] N.B. Mc Keown, Phthalocyanine materials: synthesis, Structure and Function, Cambridge University Press, Cambridge, 1998.
[4] B.P. Rand, J.G. Xue, F. Yang, S.R. Forrest, Organic solar cells with sensitivity extending into the near infrared, ApplPhys Lett 87 (2005) 233508–233508.
[5] G.A. Melson, in: Coordination Chemistry of Macro Cyclic Compounds, Plenum Press, New York, 1979, pp. 461–512.
[6] W. Song, C. He, Y. Dong, W. Zhang, Y. Gao, Y. Wu, Z. Chen, The effects of central metals on the photophysical and nonlinear optical properties of reduced graphene oxide–metal (II) phthalocyanine hybrids, Phys. Chem. Chem. Phys. 11 (2015) 7149–7157.
[7] T.V. Dubinina, P.I. Tychinsky, N.E. Borisova, V.I. Krasovskii, A.S. Ivanov, S.V. Savilov, L.G. Tomilova, Lanthanide (III) complexes of 3-(ethylthio) phenyl-substituted phthalocyanines: synthesis and physicochemical properties, Dyes and Pig 156 (2018) 386–394.
[8] N. Nwaji, B. Jones, J. Mack, D.O. Oluwole, T. Nyokong, Nonlinear optical dynamics of benzothiazole derivatized phthalocyanines in solution, thin films and when conjugated to nanoparticles, J. Photochem. and Photobio. A: Chem. 346 (2017) 46–59.
[9] a) T. Nyokong, Effects of substituents on the photochemical and photophysical properties of main group metal phthalocyanines, Coord. Chem. Rev. 251 (2007) 1707–1722; b) M. Göksel, Synthesis of asymmetric zinc (II) phthalocyanines with two different functional groups & spectroscopic properties and photodynamic activity for photodynamic therapy, Bioorg. & Med. Chem. 24 (2016) 4152–4164.
[10] T. Nyokong, Effects of substituents on the photochemical and photophysical properties of main group metal phthalocyanines, Coord. Chem. Rev. 25 (2007) 1707–1722.
[11] A. Günsel, A.T. Bilgiçli, B. Barut, P. Taslimi, A. Özel, İ. Gülçin, Z. Biyiklioğlu, M.N. Yarasir, Synthesis of water soluble tetra-substituted phthalocyanines: investigation of DNA cleavage, cytotoxic effects and metabolic enzymes inhibition, J. Mol. Struct. 1214 (2020) 128210.
[12] C. Kantar, H. Akal, B. Kaya, F. Islamoglu, M. Türk, S. Şaşmaz, Novel phthalocyanines containing resorcinol azo dyes; synthesis, determination of pKa values, antioxidant, antibacterial and anticancer activity, J. Organomet. Chem. 783 (2015) 28–39.
[13] J. Szymczak, L. Sobatta, J. Dlugaszewska, M. Kryjewski, J. Mielcarek, Menthol modified zinc(II) phthalocyanine regioisomers and their photoinduced antimicrobial activity against Staphylococcus aureus, Dyes and Pigm 193 (2021) 109410.
[14] T. Arslan, N. Çakır, T. Keleş, Z. Biyiklioglu, M. Senturk, Triazole substituted metal-free, metallo-phthalocyanines and their water-soluble derivatives as potential cholinesterases inhibitors: design, synthesis and in vitro inhibition study, Bioorg. Chem. 90 (2019) 103100.
[15] F. Özen, A. Günel, A. Baran, DNA-binding, enzyme inhibition, and photochemical properties of chalcone-containing metallophthalocyanine compounds, Bioorg. Chem. 81 (2018) 71–78.
[16] E. Dube, N. Nwaji, J. Mack, T. Nyokong, The photophysicochemical behavior of symmetric and asymmetric zinc phthalocyanines, surface assembled onto gold nanotriangles, New J. Chem. 42 (2018) 14290–14299.
[17] Ü. Demirbaş, M. Pişkin, R. Bayrak, M. Durmuş, H. Kantekin, Zinc (II) and lead (II) phthalocyanines bearing thiadiazole substituents: synthesis, characterization, photophysical and photochemical properties, J. Mol. Struct. 1197 (2019) 594–602.
[18] Y. Hu, C.Y. Li, X.M. Wang, Y.H. Yang, H.L. Zhu, 1,3,4-Thiadiazole: synthesis, reactions, and applications in medicinal, agricultural, and materials chemistry, Chem. Rev. 114 (2014) 5572–5610.
[19] N. Kushwaha, S.K.S. Kushwaha, A.K. Rai, Biological activities of thiadiazole derivatives: a review, Int. J. Chem. Tech. Res. 4 (2011) 517–531.
[20] B.A. Baviskar, S.S. Khadabadi, S.L. Deore, Synthesis and Evaluation of Some New Thiazolidin-4-One Derivatives as Potential Antimicrobial Agents, J. Chem. (2013) 1–6.
[21] a) A.M. das Neves, G.A. Berwaldt, C.T. Avila, T.B. Goulart, B.C. Moreira, T.P. Ferreira, W. Cunico, Synthesis of thiazolidin-4-ones and thiazinan-4-ones from 1-(2-aminoethyl) pyrrolidine as acetylcholinesterase inhibitors, J. Enzyme İnhibition and Med. Chem. 35 (2020) 31–41; b) A. Aktaş, M. Durmuş, İ. Değirmencioğlu, Self-assembling novel phthalocyanines containing a rigid benzothiazole skeleton with a 1, 4-benzene linker: synthesis, spectroscopic and spectral properties, and photochemical/photophysical affinity, Polyhedron 48 (2012) 80–91; c) P. Khoza, E. Antunes, T. Nyokong, Synthesis and photophysicochemical properties of zinc phthalocyanine derivatized with benzothiazole or carbazole photosensitizers, Polyhedron 61 (2013) 119–125; d) W.P. Hu, Y.K. Chen, C.C. Liao, H.S. Yu, Y.M. Tsai, S.M. Huang, J.J. Wang, Synthesis, and biological evaluation of 2-(4-aminophenyl) benzothiazole derivatives as photosensitizing agents, Bioorg. Med. Chem. 18 (2010) 6197–6207.

[22] Z. Alım, Z. Köksal, M. Karaman, Evaluation of some thiophenebased sulfonamides as potent inhibitors of carbonic anhydrase I and II isoenzymes isolated from human erythrocytes by kinetic and molecular modelling studies, Pharma. Report. 72 (2020) 1738–1748.
[23] C.T. Supuran, Therapeutic applications of the carbonic anhydrase inhibitors, Theraphy 4 (2007) 355–378.
[24] S. Kumar, S. Rulhania, S. Jaswal, V. Monga, Recent advances in the medicinal chemistry of carbonic anhydrase inhibitors, Euro. J. Med. Chem. 209 (2021) 112923.
[25] M.A. Pinard, B. Mahon, R. McKenna, Probing the Surface of Human Carbonic Anhydrase for Clues towards the Design of Isoform Specific Inhibitors, Biomed. Res. Inter. (2015) 453543.
[26] S. Ghorai, S. Pulya, K. Ghosh, P. Parthasarathi, G. Balaram, G. Shovanlal, Structure-activity relationship of human carbonic anhydrase-II inhibitors: detailed insight for future development as anti-glaucoma agents, Bioorg. Chem. (2020) 103557.
[27] T.J. Wolfensberger, The role of carbonic anhydrase inhibitors in the management of macular edema, Doc Ophthal 97 (1999) 387–397.
[28] C.T. Supuran, Applications of carbonic anhydrases inhibitors in renal and central nervous system diseases, Expert Opin. Therap. Patent. 28 (2018) 713–721.
[29] W.S. Sly, S. Sato, X.L. Zhu, Evaluation of carbonic anhydrase isozymes in disorders involving osteopetrosis and/or renal tubular acidosis, Clinic. Biochem. 24 (1991) 311–318.
[30] M.Y. Mboge, B.P. Mahon, R. McKenna, S.C. Frost, Carbonic anhydrases: role in pH control and cancer, Metabolites 8 (2018) 19.
[31] C.T. Supuran, A. Scozzafava, Carbonic anhydrase inhibitors and their therapeutic potential, Expert Opin. Ther. Pat 10 (2000) 575–600.
[32] C.T. Supuran, A. Scozzafava, Carbonic anhydrases as targets for medicinal chemistry, Bioorg. Med. Chem. 15 (2007) 4336–4350.
[33] K. Okamoto, K. Matsumoto, R. Hille, B.T. Eger, E.F. Pai, T. Nishino, The crystal structure of xanthine oxidoreductase during catalysis: implications for reaction mechanism and enzyme inhibition, Proc. Natl. Acad. Sci. U. S. A. (2004).
[34] H. Cao, J.M. Pauff, R. Hille, X-ray crystal structure of a xanthine oxidase complex with the flavonoid inhibitor quercetin, J. Nat. Prod. (2014).
[35] V. Vijeesh, N. Jisha, A. Vysakh, M.S. Latha, Interaction of eugenol with xanthine oxidase: multi spectroscopic and in silico modelling approach, Spectro. Acta Part A: Mol. and Biomol. Spectr. 258 (2021) 119843.
[36] M. Sun, J. Zhao, Q. Mao, C. Yan, B. Zhang, Y. Yang, X. Dai, J. Gao, F. Lin, Y. Duan, T. Zhang, S. Wang, Synthesis and biological evaluation of 2-(4-alkoxy-3-cyano) phenylpyrimidine derivatives with 4-amino or 4-hydroxy as a pharmacophore element binding with xanthine oxidase active site, Biorg. Med. Chem. 38 (2021) 116117.
[37] A. Hunyadi, A. Martins, B. Danko, D.W. Chuang, P. Trouillas, F.R. Chang, Y.C. Wu, G. Falkay, Discovery of the first non-planar flavonoid that can strongly inhibit xanthine oxidase: protoapigenone 10 -O-propargyl ether, Tetrahedron Lett (2013).
[38] H. Zafar, M. Hayat, S. Saied, M. Khan, U. Salar, R. Malik, M.I. Choudhary, K.M. Khan, Xanthine oxidase inhibitory activity of nicotino/isonicotino hydrazides: a systematic approach from in vitro, in silico to in vivo studies, Bioorg. Med. Chem. (2017).
[39] C.M. Kerksick, M. Zuhl, Mechanisms of Oxidative Damage and Their Impact on Contracting Muscle, Antioxidants Sport Nutr (2014).
[40] J. Huang, S. Wang, M. Zhu, J. Chen, X. Zhu, Effects of genistein, apigenin, quercetin, rutin and astilbin on serum uric acid levels and xanthine oxidase activities in normal and hyperuricemic mice, Food Chem. Toxicol. (2011).
[41] H. Matsuo, K. Ichida, T. Takada, A. Nakayama, H. Nakashima, T. Nakamura, Y. Kawamura, Y. Takada, K. Yamamoto, H. Inoue, Y. Oikawa, M. Naito, A. Hishida, K. Wakai, C. Okada, S. Shimizu, M. Sakiyama, T. Chiba, H. Ogata, K. Niwa, M. Hosoyamada, A. Mori, N. Hamajima, H. Suzuki, Y. Kanai, Y. Sakurai, T. Hosoya, T. Shimizu, N. Shinomiya, Common dysfunctional variants in ABCG2 are a major cause of early-onset gout, Sci. Rep (2013).
[42] Y.X. Hou, S.W. Sun, Y. Liu, Y. Li, X.H. Liu, W. Wang, S. Zhang, W. Wang, An improved method for the synthesis of butein using $SOCl_2$/ETOH as catalyst and deciphering its inhibition mechanism on xanthine oxidase, Molecules (2019).
[43] L. Zhang, S. Wang, M. Yang, A. Shi, H. Wang, Q. Guan, K. Bao, W. Zhang, Design, synthesis and bioevaluation of 3-oxo-6-aryl-2,3-dihydropyridazine-4-carbohydrazide derivatives as novel xanthine oxidase inhibitors, Biorg. Med. Chem. 27 (2019) 1818–1823.
[44] R. Kumar, G. Joshi, H. Kler, S. Kalra, M. Kaur, R. Arya, Toward an understanding of structural insights of xanthine and aldehyde oxidases: an overview of their inhibitors and role in various diseases, Med. Res. Rev. 38 (2018) 1073–1125.
[45] C.M. Burns, R.L. Wortmann, Gout therapeutics: new drugs for an old disease, The Lancet 377 (2011) 165–177.
[46] K. Matsumoto, K. Okamoto, N. Ashizawa, T. Nishino, FYX-051: a novel and potent hybrid-type inhibitor of xanthine oxidoreductase, J. Pharmacol Exp. Ther. 336 (2011) 95–103.
[47] C. Kantar, V. Mavi, N. Baltaş, F. İslamoğlu, S. Şaşmaz, Novel zinc(II)phthalocyanines bearing azo-containing schiff base: determination of pKa values, absorption, emission, enzyme inhibition and photochemical properties, J. Mol. Struct. 1122 (2016) 88–99.
[48] D. Aydin, E. Karakilic, S. Karakurt, A. Baran, Thiazolidine based fluorescent chemosensors for aluminum ions and their applications in biological imaging, Spectr. Acta Part A: Mol. Biomol. Spectr. 238 (2020) 118431.
[49] G. Shanlei, L. Dongni, G. Bo, L. Yanhui, Z. Haotian, L. Yanwei, D. Qian, Synthesis and catalytic performance of a soluble asymmetric zinc phthalocyanine, J. Coord. Chem. (2019).
[50] U.K. Laemmli, Cleavage of structural proteins during the assembly of the head of bacteriophage T4, Nature 227 (1970) 680–685.
[51] J.A. Verpoorte, S. Mehta, J.T. Edsall, Esterase activities of human carbonic anhydrases B and C, J. Biol. Chem. 242 (1967) 4221–4229.
[52] C. Turkes, M. Arslan, Y. Demir, D. Çoçajd, A.R. Nixhad, Ş. Beydemir, Synthesis, biological evaluation and in silico studies of novel N-substituted phthalazine sulfonamide compounds as potent carbonic anhydrase and acetylcholinesterase inhibitors, Bioorg. Chem. 89 (2019) 103004.
[53] T. Noro, Y. Oda, T. Miyase, A. Ueno, S. Fukushima, Inhibitors of xanthine oxidase from the flowers and buds of Daphne genkwa, Chem. Pharm. Bull. 31 (1983) 3984–3987.
[54] A. Baran, S. Çol, E. Karakılıç, F. Özen, Photophysical, photochemical and DNA binding studies of prepared phthalocyanines, Polyhedron (2019).
[55] a) C. Piechocki, J. Simon, Synthesis of a polar discogen, A new type of discotic mesophase, J. Chem. Soci. Chem. Com 5 (1985) 259–260; b) S.V. Kudrevich, H. Ali, J.E. Van Lier, Syntheses of monosulfonated phthalocyanines, benzonaphthoporphyrazines and porphyrins via the Meerwein reaction, J. Chem. Soc. Perkin Trans. 1 19 (1994) 2767–2774; c) J. Vacus, G. Memetzidis, P. Doppelt, J. Simon, The synthesis of unsymmetrically functionalized platinum and zinc phthalocyanine complexes, J. Chem. Soc. Chem. Com. 6 (1994) 697–698; d) T.G. Linssen, K. Dürr, M. Hanack, A. Hirsch, A green fullerene: synthesis and electrochemistry of a Diels–Alder adduct of fullerene with a phthalocyanine, J. Chem. Soc. Chem. Com. 1 (1995) 103–104; e) H. Kliesch, A. Weitemeyer, S. Müller, D. Wöhrle, Synthesis of phthalocyanines with one sulfonic acid, carboxylic acid, or amino group, Liebigs Annalen (1995) 1269–1273; f) M. Aoudia, G. Cheng, V.O. Kennedy, M.E. Kenney, M.A. Rodgers, Synthesis of a series of octabutoxy-and octabutoxybenzophthalocyanines and photophysical properties of two members of the series, J. American Chem. Soc. 119 (1997) 6029–6039.
[56] G. de la Torre, C.G. Claessens, T. Torres, Phthalocyanines: the need for selective synthetic approaches, Euro. J. Org. Chem. 16 (2000) 2821–2830.
[57] Ö. Göktuğ, T. Soganci, M. Ak, M.K. Şener, Efficient synthesis of EDOT modified ABBB-type unsymmetrical zinc phthalocyanine: optoelectrochromic and glucose sensing properties of its copolymerized film, New J. Chem. 41 (2017) 14080–14087.
[58] S. Şahin, E. Ağar, A_3B type unsymmetrical and amphiphilic phthalocyanines: synthesis, characterization, thermal stability and aggregation studies, Spectro. Acta Part A: Mol. Biomol. Spectr. 227 (2020) 117694.
[59] Ü. Demirbaş, R. Bayrak, G. Dilber, E. Menteşe, H.T. Akçay, Novel Triazole Substituted Phthalocyanines Showing High Singlet Oxygen Quantum Yields, J. Lumin (2018).
[60] Ü. Demirbaş, Novel peripherally tetra substituted phthalocyanines: synthesis, characterization, photophysical and photochemical properties, J. Mol. Struct. (2020) 128082.
[61] A.T. Bilgiçli, H.G. Bilgiçli, A. Günsel, H. Pişkin, B. Tüzün, M.N. Yarasir, M. Zengin, The new ball-type zinc phthalocyanine with SS bridge; Synthesis, computational and photophysicochemical properties, J. Photochem. and Photobio. A: Chem. 389 (2020) 112287.
[62] Y. Zorlu, F. Dumoulin, M. Durmuş, V. Ahsen, Comparative studies of photophysical and photochemical properties of solketal substituted platinum(II) and zinc(II) phthalocyanine sets, Tetrahedron 66 (2010) 3248–3258.
[63] G. Dilber, M. Durmuş, H. Kantekin, Non-aggregated zwitterionic Zinc(II) phthalocyanine complexes in water with high singlet oxygen quantum yield, Dyes and Pigm 160 (2019) 267–284.
[64] M. Durmuş, T. Nyokong, Photophysicochemical and Fluorescence Quenching Studies of Benzyloxyphenoxy Substituted Zinc Phthalocyanines, Spectrochim. Acta A 69 (2008) 1170–1177.
[65] Y. Yılmaz, J. Mack, M.K. Şener, M. Sönmez, T. Nyokong, Photophysical and Photochemical Properties and TD-DFT Calculations of Novel Highly Soluble Zinc and Platinum Phthalocyanines, J. Photochem. Photobio. A: Chem. 277 (2014) 102–110.
[66] a) N. Nombona, W. Chidawanyika, T. Nyokong, Spectroscopic and physicochemical behavior of magnesium phthalocyanine derivatives mono-substituted with a carboxylic acid group, J. Mol. Struct. 1012 (2012) 31–36; b) J. Mack, M.J. Stillman, Assignment of the optical spectra of metal phthalocyanines through spectral band deconvolution analysis and ZİNDO calculations, Coordin. Chem. Rev. 219 (2001) 993–1032.
[67] W. Spiller, H. Kliesch, S.HackbarthH. D.W¨ohrle, B. R¨oder, G. Schnurpfeil, Singlet oxygen quantumyields of different photosensitizers in polar solvents and micellar solutions, J. Porphy. and Phthalocyanines. 2 (1998) 145–158.
[68] Ü. Demirbas, C. Gol, B. Barut, R. Bayrak, M. Durmus¸, H. Kantekin, I. Degirmencioglu, Peripherally and non-peripherally tetra-benzothiazole substituted metal-free, zinc(II) and lead(II) phthalocyanines: synthesis, characterization, and investigation of photophysical and photochemical properties, J. Mol. Struct. 1130 (2017) 677–687.

[69] a) A. Nas, G. Dilber, M. Durmus, H. Kantekin, The influence of the various central metals on photophysical and photochemical properties of benzothiazolesubstituted phthalocyanines, Spectrochim. Acta 135 (2015) 55–62; b) Ü. Demirbaş, Synthesis, Characterization, Photophysical and Photochemical Properties of Novel Phthalocyanines, ChemistrySelect 5 (2020) 4530–4537.
[70] Ü. Demirbas, M. Pis¸kin, R. Bayrak, D. Ünlüer, E. Dügdü, M. Durmus¸, H. Kantekin, The determination of photophysical and photochemical parameters of novel metal-free, zin(II) and lead(II) phthalocyanines bearing 1,2,4- triazole groups, Synthetic. Met. 219 (2016) 76–82.
[71] I. Gurol, M. Durmus, V. Ahsen, T. Nyokong, Synthesis, photophysical and photochemical properties of substituted zinc phthalocyanines, Dalton Trans 34 (2007) 3782–3791.
[72] A. Ogunsipe, T. Nyokong, Photophysical and photochemical studies of sulphonated non-transition metal phthalocyanines in aqueous and non-aqueous media, J. Photochem. Photobio. A 173 (2005) 211–220.
[73] I. Seotsanyana-Mokhosi, N. Kuznetsova, T. Nyokong, Photochemical studies of tetra-2,3-pyridinoporphyrazines, J. Photochem. Photobio A 140 (2001) 215–222.
[74] M. Durmuş, in: Photochemical and Photophysical Characterization in Photosensitizers in medicine, environment, and Security, Springer, New York, 2012, pp. 135–266.
[75] J. Chenb, Q. Yec, X. Yua, X. Chena, Q. Guoa, X. Lia, H. Yangb, S. Xieb, Y. Penga, Fluorinated coumarin silicon(IV) /zinc(II) phthalocyanines: synthesis, photophysical properties and photoinduced intramolecular energy transfer, J. Lumin. 203 (2018) 299–304.
[76] E. Güzel, A. Günsel, A.T. Bilgiçli, G.Y. Atmaca, A. Erdogmus, M.N. Yarasir, Synthesis and photophysicochemical properties of novel thiadiazolesubstituted zinc(II), gallium (III) and silicon (IV) phthalocyanines for photodynamic therapy, Inorg. Chim. Acta 467 (2017) 169–176.
[77] J. Rose, Advanced Physico-Chemical experiments: a Textbook of Practical Physical Chemistry and Calculations, J. Wiley. Pitman, London, UK, 1964.
[78] Y. Derin, R.F. Yılmaz, İ.H. Baydilek, V.E. Atalay, A. Özdemir, A. Tutar, Synthesis, electrochemical/photophysical properties and computational investigation of 3, 5-dialkyl BODIPY fluorophores, Inorg. Chim. Acta 482 (2018) 130–135.
[79] B. Yıldız, E. Güzel, N. Menges, İ. Şişman, M.K. Şener, Pyrazole-3-carboxylic acid as a new anchoring group for phthalocyanine-sensitized solar cells, Solar Energy 174 (2018) 527–536.
[80] A.C. Boni, A. Wong, R.A.F. Dutra, M.D.P.T. Sotomayor, Cobalt phthalocyanine as a biomimetic catalyst in the amperometric quantification of dipyrone using FIA, Talanta 85 (2011) 2067–2073.
[81] A. Nas, H. Kantekin, A. Koca, Electrochemical and Spectroelectrochemical Analysis of 4-(4-(5-Phenyl-1, 3, 4-oxadiazole-2-yl) phenoxy)-Substituted Cobalt (II), Lead (II) and Metal-Free Phthalocyanines, Electroanalysis 27 (2015) 1602–1609.
[82] E. Güzel, Ş. Çetin, A. Günsel, A.T. Bilgiçli, İ. Şişman, M.N. Yarasir, Comparative studies of photophysical and electrochemical properties of sulfur-containing substituted metal-free and metallophthalocyanines, Res. Chem. Intermed. 44 (2018) 971–989.